Investigating the molybdenum and uranium redox proxies in a modern shallow anoxic carbonate rich marine sediment setting of the Malo Jezero (Mljet Lakes, Adriatic Sea)

Elvira Bura-Nakić[a,b*], Ivan Sondi[c], Nevenka Mikac[a], Morten B. Andersen[b,d]

[a]Ruđer Bošković Institute, Department for Marine and Environmental Reaearch, Bijenička 54, Zagreb, Croatia

[b]ETH-Zürich, Department of Earth Sciences Institute of Geochemsitry and Petrology, Claussiusstrasse 25 8092 Zürich, Switzerland

[c]Faculty of Mining, Geology and Petroleum Engineering, Pierottijeva 6, University of Zagreb, Zagreb, Croatia

[d]Cardiff University, School of Earth and Ocean Sciences, Main Place Cardiff CF10 3AT, United Kingdom

Abstract

The molybdenum (Mo) and uranium (U) isotope compositions recorded in carbonate rich sediments are emerging as promising paleo-redox proxies. However, the effects of early diagenetic effects within the sediments on these isotope systems are not well constrained. We examined the Mo and U isotopic systematics in anoxic carbonate rich sediments in a semi enclosed karstic marine lake (Malo Jezero) of the Island of Mljet, Adriatic Sea.

Measurements of water column redox behavior in the lake since the 1950s, have shown a transition from anoxic-sulfidic conditions in the deeper water column to more oxic conditions and anoxia refined to the sediment and pore-waters. A 50 cm long sediment core from the deepest part of the lake, show a transition from moderate to high authigenic Mo and U accumulation with depth, consistent with the changing lake redox environment in the past. In the deep euxinic part of the core, the authigenic Mo and U are isotopically lighter and heavier, respectively, than seawater, following similar systematics as observed in other modern euxinic basins, with high, but non-quantitative, Mo and U uptake into the sediments.

Based on Bahamas bank carbonate sediments, it has been suggested that the $^{238}U/^{235}U$ ratio is ~+0.25‰ higher compared to seawater from the effects of early carbonate sediment diagenesis and this carbonate vs. seawater off-set is applicable to carbonate rich sediments across the geological past. The shallower part of lake sediment core was deposited under similar redox conditions as the Bahamas sediments, and these sediments show an average $^{238}U/^{235}U$ ratio +0.31 ± 0.01‰ (2SE) higher than seawater. Although the average $^{238}U/^{235}U$ ratios for these two carbonate rich settings are similar, caution is necessary when inferring seawater $^{238}U/^{235}U$ compositions from such sediments, as they contain U from different sources (e.g. diagenetic uptake and carbonate-bound). The Mo isotope compositions within the same Malo Jezero sediments are variable but approaches the seawater composition at low pore-water H_2S concentrations. This show the potential of using the Mo isotope composition from carbonate rich

sediments to infer the seawater composition, however, further work is required to establish the link between the Mo isotope composition and the chemistry of the pore water environment.

Keywords: molybdenum, uranium, redox proxies, carbonate sediments, isotopes

1. Introduction

Reconstructing the chemistry and redox state of the ocean in the past is critical for understanding the evolution of life (e.g. Chen et al. 2015; Dahl et al. 2010; Lyons et al. 2014). Marine sediments provide geochemical records for such reconstruction. The reliability of identifying good indicators of specific environmental condition (i.e., proxies), and the processes controlling sequestration from an aqueous phase into the sediments, are key points in the "reconstruction chain". The enrichment of several redox-sensitive trace elements, as well as their isotopic composition (e.g. Fe, Mo, Cr, U) in (anoxic) sediments have previously shown to carry important information about the redox-sensitive mechanism of seawater removal and addition to sediments at the time of deposition (e.g. Anbar and Rouxel, 2007; Chen et al. 2015; Dahl et al. 2010; Lyons et al. 2014, Montoya-Pino et al. 2010; Planavsky et al. 2014). Yet, to fully capitalize on the potential of these emerging redox-sensitive proxies for past environments, a thorough understanding of the behavior in modern environments is mandatory.

The contrasting $^{238}U/^{235}U$ ratio (reported as $\delta^{238}U$ the $^{238}U/^{235}U$ ratio relative to the CRM 145 standard; Andersen et al. 2017) in different marine redox environments showed the promise of $\delta^{238}U$ as a tool to investigate the history of ocean oxygenation at a global scale (Weyer et al. 2008). Both organic-rich sediments and carbonates have been used to reconstruct past variations in oceanic $\delta^{238}U$, assuming a quantifiable relationship between the $\delta^{238}U$ in the geological archive and seawater (e.g. Brennecka et al. 2011; Dahl et al. 2014; Montoya-Pino et al. 2010). Early determination of $\delta^{238}U$ in modern and fossil carbonates suggested that these materials captured $\delta^{238}U$ identical to seawater (Stirling et al. 2007; Weyer et al. 2008). Further work showed, however, in addition to minor isotope fractionation effects from U incorporation into some carbonates, early diagenetic U addition from anoxic pore-waters may occur and increase the $\delta^{238}U$ in carbonate rich sediments (e.g. Chen et al. 2016; Chen et al. 2018; Romaniello et al. 2013; Tissot et al. 2018). Consequently, correction factors of +0.27 ± 0.14‰ and +0.24 ± 0.06‰, respectively, were suggested in order to estimate seawater $\delta^{238}U$ from bulk carbonate sediment $\delta^{238}U$ compositions (Chen et al. 2018; Tissot et al. 2018).

The Mo isotopic composition (reported as $\delta^{98}Mo$, the $^{98}Mo/^{95}Mo$ ratio relative to NIST SRM = +0.25‰; Naegler et al. 2014) of organic-rich sediments are used extensively in order to investigate the history of ocean oxygenation (e.g. Arnold et al. 2004; Chen et al. 2015; Dahl, et al. 2010; Dickson et al. 2014; Goldberg et al. 2016; Siebert et al. 2003). Early high-precision Mo isotope work showed large Mo isotope fractionations in marine Fe-Mn oxides, while near-quantitative Mo removal under strongly euxinic (anoxic+sulfidic) conditions in modern Black Sea yielded $\delta^{98}Mo$ near the seawater composition (+2.3‰) in deposited sediments. This led to the framework that the oceanic $\delta^{98}Mo$ is largely controlled by the size of the oxidized seafloor and Mn oxide burial, while euxinic sediment archives may record the seawater composition (Barling et al.

2001; Siebert et al. 2003; Nägler et al. 2011). Additional work showed lower δ^{98}Mo than seawater in organic rich sediments at lower H_2S water column levels, with potential additions of Mo with low δ^{98}Mo from particulate water-column shuttle processes (e.g. Arnold et al. 2004; Bura-Nakić et al. 2018; Goldberg et al. 2012; Poulson et al. 2006; Noordmann et al. 2015; Poulson Brucker et al. 2009; Scholz et al. 2017). This add uncertainty when δ^{98}Mo in ancient organic-rich sediments is used to reconstruct ocean oxygenation in the past (Arnold et al. 2004; Barling et al. 2001; Chen et al. 2015; Kendall et al. 2017; Siebert et al. 2003). It has also been suggested that non-skeletal carbonates may directly record the δ^{98}Mo of the seawater (Vogelin et al. 2009; Vogelin et al. 2010, Czaja et al. 2012). However, the Mo concentration in carbonates are generally low and potentially influenced by early diagenetic conditions within carbonate rich sediments, emphasizing the need to evaluating the processes that effect Mo and its isotopic composition during sedimentation and subsequent burial (Romaniello et al. 2016).

Coupling the Mo and U isotope redox proxies may provide a better understanding of local vs. global sedimentary δ^{238}U and δ^{98}Mo signatures (e.g. Andersen et al. 2018; Asael et al. 2013; Bura-Nakić et al. 2018; Kendall et al. 2015; Noordmann et al. 2015). For example, organic rich sediments from modern restricted euxinic basins show systematic δ^{238}U vs. δ^{98}Mo co-variation, suggested to be dominantly driven by the H_2S concentration and deep-water overturning rates (Andersen et al. 2018; Bura-Nakić et al. 2018). In this study the Mo and U concentrations and isotope systematics were investigated in modern to near-modern carbonate rich sediments from the marine lake Malo Mljet, Croatia. The deeper part of the seawater-supplied lake has shown variable redox and oxic conditions in the recent past (Lojen et al. 2010; Sondi and Juračić, 2010; Sondi et al. 2016) offering the potential to study U and Mo uptake under changing redox states in a carbonate-dominated sediment matrix. This setting therefor serves as an important analog for examining ancient carbonate sediment archives and the further understanding and utility of the combined Mo and U isotope proxies.

2. Study area

The seawater-fed lakes “Malo Jezero” and “Veliko Jezero” (“small” and “big” lake) are located on the western part of Mljet island, in the southern Adriatic Sea (Figure 1). The Mljet island is separated from the mainland by the 8-10 km wide Mljet Canal and Veliko Jezero is connected to the open sea through a shallow channel (‘Soline’ ~2.5 m depth) while another channel (~0.6 m depth) connects Veliko and Malo Jezero (Lojen et al. 2010; Sondi and Juračić, 2010; Sondi et al. 2017). Malo and Veliko Jezero are classified as doline lakes, formed as semi-closed depressions in highly permeable limestone karst of Cretaceous age (Schubert, 1909). The karstic depressions, formed during the Mesozoic, have been filled with marine waters since post-glacial sea level rise that intruded seawater through the karst. These submarine karstic connections are found to be active today, detected from sub-bottom echo profiles (Wunsam et al. 1999). Malo Jezero has a surface area of 0.25 km^2 with a maximal depth of approx. 30 m, while Veliko Jezero has a surface area of 1.45 km^2 and a maximal depth of approx. 46 m (Benović et al. 2000).

Previous studies showed that anhydrous carbonate dominate the mineral composition of the Malo and Veliko Jezero sediments with abundance up to ~70% within Malo Jezero (Lojen et al. 2010; Sondi et al. 2017; Vuletić, 1953; Figure 2). The ratio between aragonite and calcite calcium

carbonate polymorphs in the sediment varies, with aragonite the most abundant comprising approximately 60% of total Malo Jezero carbonates, defining the Mljet Lakes system as a site of distinctive authigenic aragonite formation (Sondi and Juračić, 2010; Sondi et al. 2017).

Hydrographic data for Malo Jezero has been reported since the 1950s (e.g. Vuletić 1953; Buljan and Špan 1976; Benović et al. 2001; Cuculić et al. 2008; Sondi and Jurčić 2010; Vilibić et al. 2010). The pH of the Malo Jezero waters varies between the yearly seasons with lowest pH values during winter (e.g. 8.02 ± 0.01 at the surface in January 2008), and highest pH values during summer (e.g. 8.30 ± 0.01 at the surface in July 2005). In the early 1950s the salinity in Malo Jezero bottom waters was in the range of 36-38 while surface waters were characterized by lower salinity ~29 (Buljan and Špan, 1976). An increase in salinity was noticed in the 1990s with the Malo Jezero bottom waters surpassing salinity of 38.5 (Benović et al. 2000). Spatial and temporal variations of water temperature in the Malo Jezero show typical seasonal variability, reflecting the air temperature changes, with the surface Malo Jezero waters being colder during the winter and warmer during the summer, compared to Adriatic open sea waters. A thermocline appears in early summer, deepening towards early autumn before vanishing during the winter. Records from 1997 to 1999 showed that in the summer months the thermal stratification occurred in the layers between 10-15 m (Malo Jezero) and 15-20 m (Veliko Jezero). During the periods of thermal stratification, the bottom water layers were low in oxygen, with oxygen saturation reaching minimum of 4% (Malo Jezero) and 17% (Veliko Jezero) in October 1997 (Benović et al. 2000).

Anoxic and euxinic conditions in the water column of Malo and Veliko Jezero has not been observed within the last couple of decades (Jasprica et al. 1995; Benovic et al. 2000). However, vertical sediment profiles of redox sensitive elements within Malo Jezero, indicate the occurrence of euxinic conditions in the bottom water layer of Malo Jezero and a rapid disappearance of such conditions later in the lake history (Sondi et al. 2017). Reported [H_2S] (Buljan and Špan, 1976) at 25 m water depth for the 1951 to 1961 period were in the range from 6 to 155 μmol l^{-1}, showing seasonal variations with the highest [H_2S] during the winter-autumn period (Supplementary Information Table 1). Also, the lake [H_2S] data shows that the extent of anoxia was variable, with the chemocline rising upwards during the winter-autumn period. The variable extent of anoxia is likely linked to the degree of Malo Jezero water mass exchange with Veliko Jezero and the open sea during the year. Sudden environmental change took place in the early 1960s, as a consequence of the enlargement and deepening of the Soline Channel at that time. This resulted in significantly increased water exchange between the open ocean and the lakes with the disappearance of euxinic conditions in Malo Jezero and occurrence of oxic conditions in the bottom waters as determined in July 1961 (Buljan and Špan, 1976). The irregular occurrence of dark layers of different thickness in the laminated sediments deposited before 1960s, indicates that euxinic conditions in Malo Jezero were not permanent, but were interrupted with shorter or longer oxic to suboxic periods (Supplementary Information Table 1 - Buljan and Špan, 1976; Sondi et al. 2017).

3. Sampling

Undisturbed sediment cores up to 50 cm long were collected in Malo Jezero using an Uwitec gravity corer in the period 2007-2010 at depths of 30 meter (core C1), 22 meter (core C2) and 13 meter (core C3). In order to extract pore water from sediments, sediment cores were sectioned into 2 cm segments in a glove box under an inert nitrogen atmosphere immediately after sampling. The sampled segments were centrifuged at 4000 x g for 30 minutes and the pore water was extracted using a plastic syringe and filtered through 0.45 µm Minisart cellulose acetate (Sartorius) filters under an inert nitrogen atmosphere. The segments were then freeze-dried and stored until further geochemical analyses were performed. Samples of the surrounding rocks, Cretaceous limestone and Jurassic dolomite, and the two main types of soil samples, *terra rossa* and dark humus rich soil, were also collected. Lake water was collected using a Niskin sampler system at three different depths (0, 12 and 25 m) and stored in acid cleaned plastic bottles.

4. Methods

4.1. Sample preparation

All chemical preparation and sample analyses were performed in the isotope facilities at the Institute of Geochemistry and Petrology, Department of Earth Sciences, ETH Zürich, Switzerland, unless stated otherwise.

Water sample aliquots (~20 ml) were taken for isotope analyses, aiming for a total of 20–50 ng U and 150–250 ng Mo. Aliqouts were transferred into pre-cleaned Teflon beakers, and spiked with the IRMM–3636 ^{236}U–^{233}U double-spike (Richter et al. 2008) aiming for a 1:35 spike to sample ratio, and a ^{100}Mo–^{97}Mo double-spike (approach adapted from Siebert et al. 2001) aiming for a 1:1 spike to sample ratio. These were subsequently dried down (at ~100 °C) and prepared for isotope analyses following methods described in Bura-Nakić et al. (2018). Briefly, following the seawater drying step, a large NaCl precipitate forms. This precipitate is leached using 10 ml 7 N HCl for 24 hours, a treatment which dissolves Mo, U and other metals but minimises dissolution of NaCl. After centrifugation (3500 x g for 10 minutes) the supernatant was removed, dried down and re-dissolved in 5 ml 7N HCl in preparation for column chromatography. The recoveries of both U and Mo in the supernatant were consistently >90% using this procedure (Bura-Nakić et al. 2018).

Approximately 50–100 mg of the sediment and soil samples were dissolved for analyses. Full dissolution of samples were carried out using standard protocols for silicates, involving mixtures of HF–HNO_3–HCl and H_2O_2 in the same manner as described in Andersen et al. (2013). After drying, the samples were dissolved in 10 ml 6 N HCl. One small aliquot was taken to determine elemental concentrations while another aliquot, containing 20–50 ng U and 150–250 ng Mo, was added to pre-cleaned Teflon beakers, spiked with the U and Mo double-spikes, and left to equilibrate on a hotplate before being dried down (at ~100 °C). Samples were then re-dissolved in 5 ml 7 N HCl in preparation for column chromatography.

4.2. Column chromatography

A one step purification and U–Mo separation procedure was conducted using RE Resin (Triskem technologies) in custom-made shrink-fit Teflon columns (~0.2 ml resin reservoir) following the procedure of Bura-Nakić et al. (2018). The resin was added to the Teflon columns and pre-cleaned using 2 ml 0.1 N HCl–0.3 N HF, rinsed with MQ water, and pre-conditioned with 2 ml 7 N HCl. After the samples were loaded in 5 ml 7 N HCl, the matrix was eluted with 10 ml 1 N HCl. The Mo and U fraction were eluted from the resin and collected separately, first with 5 ml 0.2 N HCl, followed by 5 ml 0.1 N HCl–0.3 N HF, respectively. The column chromatography procedure yielded high purity Mo and U fractions with low Mo and U blanks (<13 pg and <22 pg for Mo and U, respectively; Bura-Nakić et al. 2018). Prior to mass spectrometry, the U fractions were dried down and fluxed on a hotplate for 24 hours in a 1 ml 1:1 mixture of concentrated HNO_3 and H_2O_2, while the Mo fractions were merely dried down. The purified Mo and U were then re-dissolved in 1 ml 0.3 N HNO_3 and 1 ml 0.2 N HCl, respectively, for mass spectrometry. The column separation and purification procedure was tested by processing two open Atlantic Ocean samples, with measured Mo and U isotopic compositions in good agreement with previously reported values.

4.3. Elemental concentration measurements

The concentrations of selected elements (see Supplementary Information Tables 2 and 3) were measured in 0.3 N HNO_3 using a Thermo–Finnigan Element XR ICP–MS in both low and medium resolution mode, following measurement protocols in Andersen et al. (2013, 2016). A primary in-house concentration standard was interspersed with three unknowns and a secondary standard (BCR–2) was used to monitor the accuracy and reproducibility of the method. Repeated measurements of BCR–2 gave reproducibilities better than ± 10% (1 S.D.) and mean values within ± 10% of certified concentrations (see Andersen et al. 2016).

4.4. Molybdenum and uranium isotope measurements

Isotope ratios were measured on a Neptune (Thermo–Finnigan) MC–ICPMS equipped with an AridusII, auto-sampler (CETAC) using a PFA nebulizer and spray chamber (CPI) sample introduction system. Instrumental set-up details are given in Archer and Vance (2008) for Mo isotopes and Andersen et al. (2016) for U isotopes. Analysis of spiked in-house CPI standard (standard/spike ratios in the range of 0.1 to 5) as well as the open-ocean seawater were used to test the reproducibility and accuracy of the Mo isotope method. The long-term average and ±2 S.D. reproducibility during the period of this study, gave δ^{98}Mo = -0.02± 0.04‰ relative to NIST SRM = +0.25‰ (Bura-Nakić et al. 2018). Analysed seawater samples gave δ^{98}Mo of +2.37 ± 0.03‰, in agreement with previous data for seawater δ^{98}Mo (e.g. Nakagawa et al. 2012). In addition to $^{238}U/^{235}U$, $^{234}U/^{238}U$ ratios were measured and reported as ($^{234}U/^{238}U$) activity ratios (using half-lifes of Cheng et al. 2013).The verification of the U double spike method was carried out via repeated measurement of the in-house CZ–1 uraninite standard and open-ocean seawater samples. The long-term average and ±2 S.D. reproducibility for the CZ–1 standard were –0.04 ± 0.07‰ for δ^{238}U and 0.9996 ± 0.0025 for ($^{234}U/^{238}U$) (Bura-Nakić et al. 2018), in agreement with previously reported values (Andersen et al. 2016; Stirling et al. 2007). Uranium isotopic analysis of five seawater samples gave a δ^{238}U = –0.39 ± 0.04‰ and $(^{234}U/^{238}U)_{act}$ = 1.147 ± 0.003 (Bura-Nakić et al. 2018), again in very good agreement with reported data for seawater (Andersen et al.

2010, 2014; Tissot and Dauphas, 2015; Weyer et al. 2008). See Bura-Nakić et al. 2018 and Andersen et al. (2016) for further details on methods and performance.

4.5. Other analysies

The total carbonate content was determined volumetrically with a Scheibler's apparatus (Allison and Moodie, 1965) at the Ruđer Bošković Institute in Zagreb, Croatia. Sulfide concentrations were analysed by linear sweep voltammetry (LSV) within 8 hours of sampling according to established procedures (Bura-Nakić et al. 2009; Ciglenečki et al. 2005; Ciglenečki et al. 2015) at the Ruđer Bošković Institute marine station situated near Šibenik. Electrochemical measurements were performed with μAutolab Electrochemical Instruments (EcoChemie) connected with 663VA Stand Metrohm electrode.

5. Results

5.1. Elemental concentrations

5.1.1. Sediments and pore-waters

The mineral composition of sediment cores taken from the lake sediments of the Malo Jezero at cores C1, C2 and C3 (Figure 1) showed a high carbonate content, dominated by authigenic aragonite (comprising ca. 70-90% of the carbonate content) with minor calcite, magnesium calcite and dolomite. The calcite and dolomite originated from surrounding source rocks of Jurassic-Cretaceous limestones and dolomites. Besides the carbonate phases the sediments also contained small amount of mica, quartz, kaolinite and framboidal pyrite. The total carbonate content within the investigated sediments is high, comprising up to ~70% in cores C1 and C2 and reaching up to ~90% in core C3. The $[Sr]_{bulk}$ is also relatively high, ranging from 3078 to 4158 μg g^{-1}. Concentrations of sedimentary organic carbon in core C1 were measured in Lojen et al. (2010) with C_{org} (wt%) varying between 1.4 to 2.1%, with the lowest C_{org} at 13 cm depth. Using marine and terrestrial $\delta^{13}C$ endmembers signatures, Lojen et al. (2010) estimated the fraction of terrestrial organic C ranging from 53 to 76%.

The distributions of typical lithogenic elements (e.g. Al, Ti and Li) display similar behavior with sediment depth. The concentrations of Al (0.38 to 6.4%), Ti (0.03 to 0.20%) and Li (0.31 to 0.46%) are generally low, but show a gradual increase with depth in each core, while the two deepest cores (C1 and C2) have higher lithogenic element concentrations than the shallower core C3 (Figure 2 and Supplementary Information Table 2).

The bulk concentrations of the investigated redox sensitive elements ($[Mo]_{bulk}$, $[U]_{bulk}$ and $[V]_{bulk}$) display somewhat contrasting behavior. The behavior of $[V]_{bulk}$ is similar to that of the lithogenic elements, with lower $[V]_{bulk}$ in core C3 compared to cores C1 and C2. Similarly, a moderate increase in $[U]_{bulk}$ (from 2.2 to 8.4 μg g^{-1}) can be observed in all three cores, this $[U]_{bulk}$ increase is intensified below the ~20 cm sediment horizon for the two deepest cores. These sediment horizons also have high $[Mo]_{bulk}$ (25 to 78 μg g^{-1}), with a sharp contrast to lower $[Mo]_{bulk}$ (2.1 to 20

298 μg g^{-1}) above the ~20 cm sediment horizon in core C1 (Figure 2 and Supplementary Information
299 Table 2).
300
301 Pore-water [H_2S] for core C1 were determined as part of the present study and combined with
302 already published pore-water data on [Mo], [U], [Fe] and [Mn] (Sondi et al. 2017; Supplementary
303 Information Table 4). The [H_2S] increase with increasing core depth (0 to 755 μmol l^{-1}) with a
304 sharp increase between the 11 to 17 cm sediment horizons, which likely correspond to the zone
305 where reactive Fe diminishes and reduced Fe is predominating in the form of pyrite (Sondi et al.
306 2017). The pore-water concentration of dissolved Fe and Mn are highest in the subsurface
307 sediment layer at 1 cm depth, reflecting the position of the oxic-anoxic boundary. The pore-water
308 [Mo] in the top sediment layer (107 nmol l^{-1}) closely match overlying bottom water [Mo] (~110
309 nmol l^{-1}), while it generally decreases and remains lower through the core (~50-90 nmol l^{-1})
310 indicating removal of Mo from the pore-waters. The [U] in the pore-waters is exhibiting significant
311 decrease (more than 50% within the subsurface layer) in comparison to the [U] in the overlying
312 bottom waters, implying substantial U removal from the pore-waters.
313
314 **5.1.2 Catchment area and lake water**
315 Major and trace element concentrations were determined in the soil (*terra rossa* and humus) as
316 well as karst host rock samples (limestone or dolomite) collected close to the lake (Supplementary
317 Information Table 3). The carbonate host rock samples are characterised by low [Sr] (92 to 392
318 μg g^{-1}) as well as low [Al] (153 to 970 μg g^{-1}), [Li] (0.24 to 1.4 μg g^{-1}) and [Ti] (7 to 49 μg g^{-1}). The
319 [Mo] within the host rock samples is low (0.14 to 0.73 μg g^{-1}), similarly to what is typically observed
320 for carbonates (Vogelin et al. 2009) while the [U] and [V] are higher (1.3 to 3.6 and 3.5 to 23 μg
321 g^{-1}, respectively). Soil samples are characterised by [Al], [Ti] and [Li] approximatelly three orders
322 of magnitude higher than the host rock samples. Compared to the host rock samples, the soil
323 samples have similar [Sr] (61 to 102 μg/g^{-1}) while [Mo] (1.4 to 4.0 μg g^{-1}), [U] (2.4 to 4.0 μg g^{-1})
324 and [V] (72 to 168 μg g^{-1}) are all higher.
325
326 The [Mo] and [U] were measured in filtered waters sampled at 0, 12 and 25 m depth. These show
327 a narrow concetration range from 103.3 to 110.2 nmol l^{-1} and 13.0 to 13.8 nmol l^{-1} for [Mo] and
328 [U], respectively, close to average open ocean compositions (Supplementary Information Table
329 5).
330
331 **5.2 Mo and U isotopic composition**
332
333 **5.2.1. Sediments**
334 The bulk sedimentary Mo isotope compositions ($\delta^{98}Mo_{bulk}$) generally increase with depth within
335 the three sediment cores (Figure 2 and Table 1). The $\delta^{98}Mo_{bulk}$ compositions in core C1 varies
336 between +1.8 to +1.4‰, apart from the top sample at 1 cm depth with a lower $\delta^{98}Mo_{bulk}$ (+1.0‰).
337 Core C2 is characterized by $\delta^{98}Mo_{bulk}$ in the range from +2.4 to +1.7‰ while core C3 shows
338 variable Mo isotope compositions, including the lowest, $\delta^{98}Mo_{bulk}$ (+1.6 to +0.7‰).
339
340 The cores exhibit limited variation in the bulk sedimentary $\delta^{238}U$ compositions ($\delta^{238}U_{bulk}$), ranging
341 from +0.03 to -0.29‰. Core C1 show the least variable $\delta^{238}U_{bulk}$ (-0.05 to -0.15‰), followed by
342 core C2 (+0.02 to -0.13‰), while core C3 have $\delta^{238}U_{bulk}$ of -0.29‰ for the top 1 cm and +0.03‰

at 23 cm depth. The $(^{234}U/^{238}U)_{act}$ for the bulk sediments increase with depth in all three cores (Figure 2 and Table 1). Cores C2 and C1 have the highest $(^{234}U/^{238}U)_{act}$ (1.065 to 1.033) while core C3 show lower $(^{234}U/^{238}U)_{act}$ (from 1.023 to 1.000 for the 1 cm depth sample).

5.2.2. Soil and water samples

The measured δ^{98}Mo (average +2.41±0.02‰), and δ^{238}U (average -0.36±0.02‰) in the Malo Jezero lake waters at 0, 12 and 25 m depth (Supplementary Information Table 5) are close to the open ocean ($\delta^{98}Mo_{Sw}$=+2.37‰ and $\delta^{238}U_{Sw}$=-0.39‰; Andersen et al. 2014; Nakagawa et al. 2012). The $(^{234}U/^{238}U)_{act}$ for the same lake water samples (1.136 to 1.138) are slightly lower than the open ocean seawater (1.147; Andersen et al. 2010). The *terra rossa* and the humus soil samples were characterized by variable $(^{234}U/^{238}U)_{act}$ (1.102 and 0.977), but similar δ^{238}U (-0.28‰ and -0.22‰) and δ^{98}Mo (+0.53‰ and +0.62‰), see Table 1.

6. Discussion

The main aim is to broaden our understanding of δ^{98}Mo and δ^{238}U signatures within carbonate rich sediments under changing redox conditions. The discussion on the sedimentary δ^{98}Mo and δ^{238}U budget therefor primarily focusses on the deep Malo Jezero sediments (core C1), due to the available literature data (Sondi et al. 2017) and the most complete δ^{98}Mo and δ^{238}U data-set.

6.1. The sources of Mo and U in the sediments of Malo Jezero

The uptake of the redox-sensitive U, Mo and V in the Malo Jezero sediments will be impacted by various biogeochemical and physical processes. Three main sources may be considered important for the sediments in this particular system; *(1)* the addition from detrital material, e.g. siliciclastic and carbonate, *(2)* the formation of authigenic carbonate phases in the lake and *(3)* other transport uptake mechanisms, either from authigenic processes directly within the waters and/or pore-water. Below, these three potential sources are discussed in turn.

(1) Sondi et al. (2017) concluded that soils were an important source of material deposited in the Veliko and Malo Jezero based on the similar geochemistry of soil and sediment from sampled cores. However, the soils surrounding the lake are heterogenous and in order to estimate the possible influence of this detrital material on the sediment geochemistry, two general detrital end-members can be defined; limestone/dolomite vs. siliciclastic (clay) dominated soils (Figure 3). These two end-members have distinct geochemical signatures. The Malo Jezero sediments shows a near-linear relationship between typical lithogenic elements (e.g. [Al] vs. [Ti] and [Al] vs. [Li]), suggesting that the Malo Jezero lithogenic fraction in the sediments are a physical mixture of the two generalised detrital end-members (Figure 3). Vanadium concentrations in the sediments also show similar mixing relationship with [Al], while both [U] and [Mo] show generally higher concentrations than can be explained by simple mixing of these two end-member sources (Figure 3). This suggests that, while the redox sensitive V are likely dominated by the detrital fraction, additional source(s) of Mo and U uptake is/are required to explain the sediment data.

(2) The mineralogy of the sediments within Malo Jezero revealed that aragonite is the dominating carbonate fraction. This source of authigenic-formed aragonite in the lake is manifested in high

sediment [Sr] (3000-5000 μg g^{-1}) compared to the soil and limestone host rocks (61 to 392 μg g^{-1}) a feature also observed in previous studies (Sondi and Juračić, 2010; Sondi et al. 2017). The authigenic-formed aragonite could provide an additional source of U and Mo to the sediments. However, marine aragonite is typically characterized by low [Mo] (Voegelin et al. 2009; Romaniello et al. 2016) and no correlation is observed between [Mo] and [Sr] (Figure 3), suggesting limited Mo addition from this source. While [U] is normally relatively high in marine aragonite (2-4 μg g^{-1} range; Dunk et al. 2002), there is no obvious correlation between [U] and [Sr] (Figure 3), suggesting that the U incorporation into this lake aragonite phase is minor. This suggests that the relatively high [Mo] and [U] observed in the deeper parts of cores C2 and C1 must be dominated by other uptake mechanism(s).

(3) Authigenic uptake of Mo and U in sediments often occur under reducing conditions. For both U and Mo, early *in-situ* diagenetic precipitation is observed in a range of environments with euxinic pore-waters (e.g. Chen et al. 2018; McManus et al. 2006; Morford et al. 2005; Romaniello et al. 2013, 2016; Zheng et al. 2002). High Mo accumulation also occur in strongly euxinic waters, presumably via the formation of sulfidic molybdate species followed by particulate organic scavenging or formation and scavenging of authigenic $FeMoS_4$ minerals (e.g. Algeo and Lyons, 2006; Erickson and Helz, 2000; Helz et al. 1996; Helz et al. 2011; Helz and Vorlicek, 2019). Other potential important sources of addition of Mo and U in anoxic sediments may be associated directly with deposited organic matter (e.g. Kowalski et al. 2013; King et al. 2018; Zheng et al. 2002) and (particularly for Mo) Fe-Mn shuttle processes (e.g. Algeo & Lyons 2006; Scholz et al. 2017). All three cores show an increase in [U] with depth (Figure 2) suggesting increasing U addition to the sediments with decreasing redox potential at depth in the pore waters. The highest [U] (>5 μg g^{-1}) is observed at depths below 20 cm in cores C1 and C2, similar to the zones of the highest [Mo] (>40 μg g^{-1}). In contrast, the [Mo] is much lower in the horizons above (<5 μg g^{-1}) and there is little evidence for any Mo addition in core C3 (Figure 2).

6.2. Quantification of the authigenic U and Mo fractions in the Malo Jezero sediments

With a general separation of the different sources of U and Mo in the sediments, it is possible to further quantify the authigenic U and Mo fractions, and associated isotope signatures, to provide better constraints on the processes governing the mechanisms of U and Mo enrichment.

The daughter ^{234}U to parent ^{238}U activity ratio, $(^{234}U/^{238}U)_{act}$ can provide an effective method to distinguish between U from an authigenic or detrital source in Holocene-aged sediments (e.g. Holmden et al. 2015; Andersen et al. 2016). This stem from modern seawater $(^{234}U/^{238}U)_{act}$ is ~15% enriched in ^{234}U due to α-recoil processes, while older detrital lithogenic material is normally characterized with a $(^{234}U/^{238}U)_{act}$ near secular equilibrium (Andersen et al. 2010). The $(^{234}U/^{238}U)_{act}$ in the surface sample of core C3 is in secular equilibrium, implying negligible authigenic U and can therefore be considered a detrital end-member. This sample is characterized by $[U]_{bulk}$ of 2.2 μg g^{-1}, U/Al ratio of 5.8 × 10^{-4} g/g and $\delta^{238}U$ of –0.29‰. This sediment sample is also characterized by high $CaCO_3$ and [Sr] suggesting that, as already discussed, the contribution of U from authigenic aragonite has a minor impact on the sedimentary U budget. Sediments with higher [U] show increasing $(^{234}U/^{238}U)_{act}$ consistent with increasing authigenic U accumulation. The sediments show a broadly linear correlation between $(^{234}U/^{238}U)_{act}$

vs. 1/[U], suggesting a mixture between detrital and authigenic U (Figure 4). However, the inferred authigenic end-member of this linear mixing line has a $(^{234}U/^{238}U)_{act}$ of ~1.09, a value significantly lower than the measured $(^{234}U/^{238}U)_{act}$ in the lake waters (~1.14). The origin of this relatively low authigenic $(^{234}U/^{238}U)_{act}$ estimation is not clear. One possibility is incongruent calcite dissolution, as suggested to occur within the reducing Malo Jezero sediments (Lojen et al. 2010), releasing U with low $(^{234}U/^{238}U)_{act}$ which then mixes with seawater-derived U in the pore-waters. Alternative suggestions may be related to additional groundwater input or dissolution of karst during seawater flow-through in cthe ave systems, both adding U with low $(^{234}U/^{238}U)_{act}$. Lower than seawater $(^{234}U/^{238}U)_{act}$ was also observed in the seawater lake Rogoznica, Croatia, which is also fed through karst cave systems (Bura-Nakić et al. 2018). Whichever the mechanism, the uncertainties in the $(^{234}U/^{238}U)_{act}$ for the both the detrital and authigenic U end-members, limits the usage of $(^{234}U/^{238}U)_{act}$ to quantify the authigenic U contribution in the Mjet lake sediments (see also section 6.4).

Instead, the authigenic to detrital components for both U and Mo can be estimated comparing these to Al, typically used for estimating authigenic enrichment factors (EF; e.g. Tribovilliard and Algeo, 2009). However, the detrital fraction of U and Mo in each sediment horizon is a mixture between the (i) limestone/dolomite and (ii) their weathering products in the form of *terra rossa* and organic richs soils (as shown by the Al vs. Ti correlation, Figure 3). Thus, using only one average [U]/[Al] or [Mo]/[Al] ratio for the detrital fraction would lead to under- and/or overestimation of the authigenic U and Mo component. Instead, to estimate the U and Mo detrital vs. authigenic contribution, a linear regression line can be estimated between the two generalized detrital end-members in the [U] or [Mo] vs. [Al] space, which reflect the degree of weathering of the detrital source (Figure 5). Using this approach, the $[U]_{auth}$ and $[Mo]_{auth}$ fractions are estimated to range between 14 to 68%, and 4 to 98% of the bulk, respectively (Table 2). Both $[Mo]_{auth}$ and $[U]_{auth}$ show progressive increases with depth in all the cores. Furthermore, both cores C2 and C1 show a large increase in $[Mo]_{auth}$ between 18 to 25 cm depth, while C3 core show much lower overall $[Mo]_{auth}$ (Figure 6). The two upper part of core C3 (1 and 9 cm depth) are characterized by very low $[Mo]_{bulk}$ (0.18 and 0.13 µg g^{-1}, respectively) close to the average carbonate catchment [Mo] (0.29 µg g^{-1}, n=5), showing the $[Mo]_{auth}$ is negligible if at all present in these sediments. The estimated $[U]_{auth}$ for the top 1 cm in core C1 is the lowest within the investigated sediments (0.33 µg g^{-1}), in agreement with the minimal authigenic U uptake based on the $(^{234}U/^{238}U)_{act}$ composition.

6.3. Estimating the authigenic U and Mo isotope signatures in the Malo Jezero sediments

The estimation of $\delta^{238}U_{auth}$ and $\delta^{98}Mo_{auth}$ build on $[U]_{auth}$ and $[Mo]_{auth}$ calculations (Figure 6). Combining the relative size of the detrital component with an estimated isotopic composition can provide an estimated isotope composition of the authigenic fraction. As the detrital fraction for each sediment sample is a mixture between the two detrital end-members, the isotope composition also needs to be estimated for each sediment sample. For U, both end-member have very similar $\delta^{238}U$ (the clay fraction of -0.28‰ and carbonate/dolomite fraction of -0.29‰, based on the 1 cm sediment sample in core C3) and both are similar to average 'bulk Earth' and continental crust $\delta^{238}U$ estimates (Andersen et al. 2017; Tissot et al. 2015). For the detrital Mo, the $\delta^{98}Mo$ of the clay fraction were estimated to be +0.58‰ (average of the measured soils) while the carbonate/dolomite fraction were estimated to be +1.03‰ (based on the 1 cm sediment

sample in core C3), both slightly higher than typically used for detrital δ^{98}Mo compositions (~0.0 to +0.3‰; Kendall et al. 2017). The $\delta^{238}U_{auth}$ and $\delta^{98}Mo_{auth}$ estimates (Figures 6 and 7 and Table 2), have uncertainties estimated based on propagated measurement errors scaled to the relative size of the detrital component (see Andersen et al. 2014 for details). This error propagation leads to increasing uncertainty estimates with increasing detrital contribution. Therefore, detrital-dominated sediments with uncertainties >0.4‰ (±2σ) on the $\delta^{238}U_{auth}$ or $\delta^{98}Mo_{auth}$ (Table 2) are deemed unreliable and omitted from figures and further discussion.

Core C1 show $\delta^{238}U_{auth}$ from +0.25‰ to -0.07‰, all significantly higher than the seawater δ^{238}U composition of -0.39‰ and with a systematic decrease in $\delta^{238}U_{auth}$ with depth and higher $[U]_{auth}$ (Figures 6 and 7). The measured sediments in core C2 and at depth in core C3 show high $\delta^{238}U_{auth}$ similar to core C1 (Figures 6 and 7). Similarly to U, $[Mo]_{auth}$ show a progressive increase with depth for core C1, with $\delta^{98}Mo_{auth}$ compositions between +1.09‰ and +2.02‰. Below ~20 cm the $\delta^{98}Mo_{auth}$ is relatively homogenous at ~+1.7‰, while above, the $\delta^{98}Mo_{auth}$ varies, including the lowest $\delta^{98}Mo_{auth}$ composition at 1 cm depth (+1.09‰). The $\delta^{98}Mo_{auth}$ varies from +1.85‰ to +2.45‰ in core C2, with samples at 37 cm and 17 cm close to the seawater δ^{98}Mo composition. In core C3 the $\delta^{98}Mo_{auth}$ can only be estimated for the two deepest samples (17cm and 24 cm) giving +1.18 and +1.72‰ (Figures 6 and 7).

6.4. Evaluating the controls on the authigenic Mo and U in the Malo Jezero sediments

The three water samples taken at different lake depths show both [U], [Mo], δ^{238}U and δ^{98}Mo very close to open-ocean seawater compositions (Supplementary Information Table 5). This shows that the lake is dominated by seawater-derived U and Mo, the authigenic Mo and U in sediments can be directly compared to the seawater. The progressive increase in $[U]_{auth}$ and $[Mo]_{auth}$ with depth in cores C1 and C2 is similar to observations in Bahamas bank carbonate sediments, where $[U]_{auth}$ and $[Mo]_{auth}$ increases have been interpreted to be from increasing organic matter respiration and buld-up of pore-water H_2S (Romaniello et al. 2013; 2016). Cores C1 and C2, however, show a clear transition around ~20 cm depth with a sharp increase in sedimentary $[Mo]_{auth}$ and $[U]_{auth}$ as well as pore-water $[H_2S]$. This increase in $[Mo]_{auth}$ and $[U]_{auth}$ at depth could be directly related *in situ* diagenetic respiration of organic matter or it may reflect an euxinic redox regime in the lake with other pathways of U and Mo uptake at the time of sediment deposition below ~20 cm depth. Correlations between $Mo]_{auth}$ and $[U]_{auth}$ vs. C_{org} may potentially help to distinguish between these two scenarios.

Positive correlations between both U vs. C_{org} and Mo vs. C_{org} have been observed in many anoxic/euxinic sediments (e.g. McManus et al. 2005; Algeo and Lyons, 2006; Wagner et al. 2017). The positive Mo vs. C_{org} correlation have been attributed to processes of Mo scavenging from seawater by organic shuttle processes (e.g. Algeo and Lyons, 2006; Wagner et al. 2017), or, alternatively, a lowering of Mo solubility in waters from microbial sulfate reduction fueling on C_{org} (e.g. Helz and Vorlicek, 2019). A similar debate exist for positive U vs. C_{org} correlations, suggested to either occur from direct U scavenging with organic material (e.g. Zheng et al. 2002) or C_{org} fueling microbial mediated metal (and U) reduction within sediments (e.g. McManus et al. 2005; Lovley et al. 1991). Available C_{org} vs. bulk [Mo] and [U] data for core C1, show no positive correlations and little variability in C_{org} with depth (Figure 8). Similarly, no U vs. C_{org} correlation

have been observed in Bahamas bank carbonate sediments (Tissot et al. 2018). In contrast, the four upper samples from core C1 (<20 cm) show weak negative correlations between [Mo] vs. C_{org} and [U] vs. C_{org} (Figure 8), in opposite direction to general observations in euxinic basins (Algeo and Lyons, 2006). If these observations are considered significant, then increased microbial metal reduction leading to higher [H_2S] and more efficient Mo and U uptake, while using up available C_{org} in the process, could be an explanation. The lack of correlation between the [Mo] vs. C_{org} in the deeper part of the core (>20cm) is consistent with the model of Helz and Vorlicek (2019) suggesting [Mo] vs. C_{org} correlations degrade where the flux of Mo is independent of the sulfate reduction process in strongly euxinic waters.

Yet in euxinic sediments, even minor U or Mo accumulation associated directly with organic matter and/or Fe-Mn oxides, may have a significant impact on the Mo and U isotope systematics as these uptake processes commonly show large isotopic fractionation (e.g. Abshire et al. 2020; Barling et al. 2004; King et al. 2018; Kowalski et al. 2013). Impact of such processes in the lake sediments can be investigated comparing $\delta^{98}Mo_{auth}$ and $\delta^{238}U_{auth}$ compositions to inverse $[Mo]_{auth}$ and $[U]_{auth}$ (Figure 9), where correlations can be attributed to mixing of different sources of authigenic Mo and U. The $\delta^{238}U_{auth}$ show little variability over a range of $[U]_{auth}$, with a general trend of slightly increasing $\delta^{238}U_{auth}$ with lower $[U]_{auth}$. This suggest little contribution, if any, of authigenic U associated directly organic matter carrying low $\delta^{238}U_{auth}$ as observed in other anoxic settings (e.g. Abshire et al., 2020; Holmden et al., 2015). Sources of authigenic U may be further explored cross-plotting $\delta^{238}U_{auth}$ vs. $[U]_{auth}/C_{org}$. Here the lake sediments show a negative correlation for samples with low $[U]_{auth}/C_{org}$ (<2) and $\delta^{238}U_{auth}$ decreasing from +0.2 to -0.05‰, while at higher $[U]_{auth}/C_{org}$ (>2), the $\delta^{238}U_{auth}$ are similar, centered around -0.05‰ (Figure 9). This relationship suggests that at high $[U]_{auth}/C_{org}$ (>2) the U uptake is dominated by *in situ* U reduction, while at lower $[U]_{auth}/C_{org}$ (<2), U associated directly with organic matter constitute a significant U fraction when compared to the *in situ* U reduction. This interpretation is consistent with the sediment data from the Namibian shelf in Abshire et al. (2020), except that in this study the U associated with organic matter has a high $\delta^{238}U_{auth}$ (~+0.2-0.4‰; Figure 9) in contrast to low $\delta^{238}U$ (~-0.6‰) in Abshire et al. (2020). The potential U source with such high $\delta^{238}U$, could be associated with detrital, rather than authigenic, organic matter and adsorption of isotopically heavy U^{+4} before transportation to the lake and sediments. Such a detrital organic U source would not be accounted for in the estimated detrital U fraction and it would provide U with low $(^{234}U/^{238}U)_{act}$ and a mechanism to lower estimated authigenic $(^{234}U/^{238}U)_{act}$ end-member (see section 6.2). For the Mo systematics, the sediments with the lowest $\delta^{98}Mo_{auth}$ compositions also correspond to the lowest $[Mo]_{auth}$ and could have significant Mo addition from organic matter and/or Fe-Mn oxides. The samples with the high authigenic $[Mo]_{auth}$ below 20 cm depth in cores C1 and C2, on the other hand, suggest one dominating authigenic $[Mo]_{auth}$ source (Figure 9). Cross-plotting $\delta^{98}Mo_{auth}$ vs. $[Mo]_{auth}/C_{org}$ show no correlation to indicate mixing between Mo associated organic matter and/or Fe-Mn oxides with low $\delta^{98}Mo_{auth}$ compared to $[Mo]_{auth}$ associated with formation and scavenging of sulfidic molybdate species or $FeMoS_4$ minerals with high $\delta^{98}Mo_{auth}$ (Figure 9).

In summary, these observations suggest that the both the U and Mo uptake is primarily related to microbial sulfate and metal reduction processes (and [H_2S] formation for Mo) within the deeper parts of cores C1 and C2. In shallower sediments with lower authigenic U and Mo uptake from

these processes, the role of organic matter scavenging and/or Fe-Mn adsorption for U and Mo may be significant contributors to the authigenic U and Mo fractions.

6.5. Coupled authigenic Mo and U and isotope systematics in the Malo Jezero sediments

With a general understanding of the dominant uptake mechanisms for U and Mo, it offers the possibility to investigate the combined behavior of the two metals in more detail (Figure 10). The modest authigenic U and Mo enrichments in sediments above ~20 cm (Figure 10 and Supplementary Information Table 6) is consistent with anoxia/euxinia predominantly confined to the pore-water of the sediments (Tribovilliard and Algeo, 2009), while the significant increase in $[Mo]_{auth}$ below ~20 cm depth (cores C1 and C2) reflect Mo and U accumulation under euxinic water conditions during sediment deposition. These interpretations align well with the observed changing redox regime from euxinic to oxic bottom waters in the lake over time. Based on the geochemical systematics, the sediments can be divided into three zones with increasing depth: *i*) a zone of Mo addition from particulate transport; *ii*) a zone of pore-water Mo and U uptake and *iii*) a deeper zone of previously water column/pore-water Mo and U uptake.

Zone *i)* shows high [Fe] and [Mn] in the pore-water profiles (Figure 11) suggesting a zone of Fe-Mn oxide addition and dissolution in the shallowest sediment (<1 cm depth). Pore-water [Mo] surrounding these sediments are close or just below seawater [Mo] (Figure 11). Molybdenum transport from an Fe-Mn particulate shuttle process (e.g. Scholz et al. 2017) is therefore a likely explanation for the relatively low $\delta^{98}Mo_{auth}$ (1.02‰) in the top 1 cm sediment. However, this sediment sample has relatively low $[Mo]_{bulk}$ (2.1 µg g^{-1}) and any Mo addition from Fe-Mn oxides can therefor only provide a small contribution to the total accumulated Mo in the sediments as also discussed in section 6.4).

Zone *ii)* the shallower <20 cm sediments in cores C2 and C1 are characterized with relatively low Mo_{EF} (0.3 to 11) and U_{EF} (1.1 to 2.3) suggesting euxinic conditions localized within the pore-waters (Figure 8). The $\delta^{238}U_{auth}$ (~+0.1 to +0.25‰) is consistent with the observed $\delta^{238}U$ range in modern sediments with variable anoxic pore-water levels (e.g. Andersen et al. 2016). The data would be consistent with permanent anoxia and a shallow oxic-anoxia boundary (low oxygen penetration) in the pore-waters with authigenic U accumulation and a $\Delta^{238}U$ ~+0.6‰ (Andersen et al. 2014; Figure 7), however, as discussed in section 6.4, U addition associated with organic matter may also be significant. The $[Mo]_{auth}$ varies between +1.0 to +2.3‰ in the same samples. Such $\delta^{98}Mo_{auth}$, lower than the seawater $\delta^{98}Mo$ composition, have been observed in reducing organic carbon-rich sediments, attributed to a range of processes including low $[H_2S]$ and incomplete thiomolybdate or $FeMoS_4$ transformation and, as discussed in section 6.4, addition of isotopically light Mo associated with organic matter deposition or a Fe-Mn shuttle process (e.g. Azrieli-Tal et al. 2013; Poulson Brucker et al. 2009; Kowalski et al. 2013; Kendall et al. 2017; Scholz et al. 2017; King et al. 2018; Helz & Vorlicek, 2019). These $\delta^{98}Mo_{auth}$ compositions are similar to observations in Bahamas bank carbonate sediments where the samples with the lowest pore-water $[H_2S]$ have low sedimentary [Mo] and $\delta^{98}Mo$ in the range from ~1.05‰ to ~1.25‰ (Romaniello et al. 2016). The negative [Mo] and [U] vs. C_{org} correlations suggest increased microbial sulfate reduction using up available C_{org} (Figure 8), a process that fits with the increasing gradient in $[H_2S]$ with depth and the observed $\delta^{238}U_{auth}$ and $\delta^{98}Mo_{auth}$ systematics. In the upper part (5 to 9 cm) with low pore-water

607 [H_2S] (0.6 to 2.1 µmol l^{-1}), the authigenic [Mo] is low, but the $\delta^{98}Mo_{auth}$ close to the seawater $\delta^{98}Mo$
608 composition. The [H_2S] is well below the threshold (~11 µmol l^{-1}) needed for the complete
609 transformation of MoO_4^{2-} to MoS_4^{2-} (Erickson and Helz, 2000). Consequently, for this type of
610 authigenic Mo uptake, Mo is expected to be incorporated into the solid phase mostly in the form
611 of MoO_4^{2-} and this process appears to be accompanied by a low levels of Mo enrichment, but with
612 little net Mo isotope fractionation. The deeper part (13 to 17 cm) is characterized by higher
613 porewater [H_2S] (29 to 200 µmol l^{-1}) and the sediments have higher authigenic [Mo], but $\delta^{98}Mo_{auth}$
614 lower than the seawater $\delta^{98}Mo$ composition. These observations are in accordance with previous
615 findings (Bura-Nakić et al., 2018) and could relate to the Mo isotope fractionation in the earliest
616 stages of Mo removal is significant and driven by [H_2S] near the action point of switch for complete
617 transformation of MoO_4^{2-} to MoS_4^{2-} or $FeMoS_4$ formation (Helz et al., 1996; Helz and Vorlicek,
618 2019; Kerl et al., 2017; Nägler et al., 2011; Tossel et al. 2005). The data within this study is
619 generally in agreement with the work of Romaniello et al. (2016) highlighting the important role of
620 [H_2S] regulating the [Mo] within the pore-waters and sedimenst. However, in contrast to the
621 observations in Romaniello et al. (2016) there is no clear trend between $[Mo]_{auth}$ vs. $\delta^{98}Mo_{auth}$, with
622 the highest $\delta^{98}Mo_{auth}$ recorded at a very low $[Mo]_{auth}$ and almost in absence of pore-water [H_2S].
623
624 Zone *iii)* the high $[Mo]_{auth}$ and $[U]_{auth}$ below 20 cm depth in both cores C2 and C1 suggest highly
625 euxinic conditions in the lake bottom- and pore-waters during sediment deposition. Bura-Nakić et
626 al. (2018) investigated combined $\delta^{98}Mo_{auth}$ vs. $\delta^{238}U_{auth}$ in another euxinic Croatian sea-water lake
627 (Rogoznica) and compared the results to organic-rich sediments from other restricted euxinic
628 basins. The deep sediments in the lake show combined $\delta^{98}Mo_{auth}$ vs. $\delta^{238}U_{auth}$ systematics that are
629 broadly similar to observations from Saanich Inlet and Cariaco Basin (Figure 10). The $\delta^{98}Mo_{auth}$
630 vs. $\delta^{238}U_{auth}$ systematics of the modern euxinic basins revealed patterns that are likely to be mainly
631 controlled by interlinked factors of basin size, [H_2S] and deep-water renewal rates (Bura-Nakić et
632 al. 2018). In this framework, strongly euxinic basins with slow deep-water renewal rates, lead to
633 near quantitative Mo uptake and nearly unfractionated Mo isotope compositions in the sediments.
634 This may, for instance, be accomplished by near complete transition from molybdate to tetra-
635 thiomolybdate and effective scavenging to the sediments. In contrast, in basins with fast deep-
636 water renewal rates, less-effective Mo scavenging lead to non-quantitative removal of Mo from
637 the water column and expressed Mo isotopes fractionations in the sediments. If the transformation
638 to tetra-thiomolybdate is incomplete, Mo scavenged to the sediments will express a $\Delta^{98}Mo$ that
639 are ~0.7‰ lower than seawater (e.g. Bura-Nakić et al., 2018; Dahl et al., 2010; Dickson; 2017).
640 Such a scenario for the Mo accumulation could be consistent with the average $\delta^{98}Mo_{auth}$ of ~1.6‰
641 in the sediments below 20 cm in core C1 (Figure 7 and 10). Core C2, below 20 cm, show similar
642 behavior as core C1 for two samples, while two other samples have higher $\delta^{98}Mo_{auth}$ near the
643 seawater composition (Figure 7). The more variable $\delta^{98}Mo_{auth}$ for core C2 may be related to a
644 position closer to the lake's chemocline and variable [H_2S] in the water column. The U uptake into
645 the organic carbon-rich sediments of euxinic basins are normally less quantitative than that of Mo,
646 expressing a $\Delta^{238}U$ of ~+0.6‰ between the reduced U in the sediments and the overlaying bottom-
647 waters (Andersen et al., 2014; Andersen et al., 2018; Bura-Nakić et al., 2018). Given a
648 predominantly U uptake from diffusion and reduction within pore-waters of the sediments, slow
649 deep-water renewal compared to U diffusion rates, may deplete U in the water column above the
650 sediments (e.g. Anderson et al., 1989; Rolison et al., 2017) and drive the waters towards lower

651 $\delta^{238}U$. The effect of slow deep-water renewal rates is that U removal becomes more quantitative
652 and the $\delta^{238}U_{auth}$ in the sediments move towards the seawater $\delta^{238}U$ composition (e.g. Andersen
653 et al., 2014; Andersen et al. 2018; Bura-Nakić et al., 2018). Thus, as with $\delta^{98}Mo_{auth}$, the $\delta^{238}U_{auth}$
654 data is fully consistent with bottom water euxinia in the deeper part of the lake, but with a relatively
655 fast deep-water overturning time compared to the basin size, leading to $\delta^{238}U_{auth}$ of ~0‰ in
656 sediments, ~0.4‰ higher than open ocean seawater $\delta^{238}U$ composition (Figure 7 and 10).
657
658 Similar interpretations as based on the Mo and U isotope systematics are, in principle, possible
659 to obtain from Mo vs. U enrichment factors (using Al normalization, see Tribovilliard et al. 2012).
660 In this study, the Al normalization was performed using the calculated detrital [U]/[Al] and [Mo]/[Al]
661 for each specific sample, based on the two detrital end-members (Supplementary Information
662 Table 6). It must be noted that, the large carbonate fraction in these sediments, have to be
663 considered when comparing these results to other sediments, richer in detrital siliciclastic material
664 (Figure 10). The observed Mo_{EF}/U_{EF} for the deep part of cores C2 and C1 are about twice as high
665 as the seawater Mo/U molar ratio, a trend often interpreted as evidence for Mo addition to
666 sediments via Fe-Mn particulate shuttle processes (e.g. Algeo and Tribovillard, 2009). However,
667 similar high Mo_{EF}/U_{EF} have also been observed for the Saanich Inlet and Cariaco Basin and the
668 combined Mo_{EF}/U_{EF} and $\delta^{98}Mo_{auth}/\delta^{238}U_{auth}$ systematics (Figure 10) are fully consistent with
669 different Mo and U removal rates within euxinic basins with relatively fast deep-water overturning
670 rates (see Bura-Nakić et al. 2018 for discussion).
671
672 **6.6. Implications for the interpretation of $\delta^{238}U$ and $\delta^{98}Mo$ in carbonate-rich sediments**
673 It is clear that the process of early diagenesis from reducing pore-water conditions within
674 carbonate-rich sediments may lead to the accumulation of authigenic U and Mo (e.g. Romaniello
675 et al. 2013, 2016). Based on Bahamas carbonate-rich sediments, Chen et al. (2018) and Tissot
676 et al. (2018) suggested a $\Delta^{238}U$ of +0.27 ± 0.14‰ and +0.24 ± 0.06‰, respectively, to be
677 applicable to derive seawater $\delta^{238}U$ estimates from measured bulk (anoxic) carbonate $\delta^{238}U$. The
678 $\Delta^{238}U$ of the carbonate sediments in this study were on average +0.29 ± 0.03‰ higher than
679 seawater. The carbonate sediments from 1 to 17 cm depth in core C1 are interpreted to have
680 been deposited under reducing pore-waters and these samples are therefore more comparable
681 with the conditions of the Bahamas bank carbonate-rich sediments. These core C1 sediments
682 have a mean $\Delta^{238}U$ of +0.31 ± 0.01‰ compared to seawater, slightly higher but within uncertainty
683 of the Bahamas carbonate-rich sediments (Cheng et al. 2018; Romaniello et al. 2013; Tissot et
684 al. 2018). Despite the similar $\Delta^{238}U$ at these different settings, it has to be noted that the observed
685 $\delta^{238}U$ in carbonate-rich sediments are a combination both detrital and authigenic U which may
686 have variable $\delta^{238}U$ and isotope fractionation factors (e.g. dependent on oxygen penetration
687 depth; Andersen et al. 2014). Another uncertainty is where the authigenic U is bound in the
688 sediments, as already discussed, the majority of the U is not associated with the authigenic-
689 formed aragonite in the Malo Jezero sediments. Instead it appears that the authigenic U is added
690 as U^{IV} with associated U isotope fractionation. Authigenic U addition in the Bahamas carbonate-
691 rich sediments has been suggested to be either in the form of reduced U mineral phases or
692 incorporated into the carbonate crystal lattice under anoxic conditions (e.g. Chen et al. 2018), but
693 further work is required to understand where this U^{IV} is hosted and its exact associated U isotope
694 fractionation in anoxic carbonate-rich settings.

Core C1 with high-resolution pore-water [H_2S] data allows to discuss the relationship between the sediment [Mo] concentration and pore-water [H_2S]. The [H_2S] within the upper 17 cm is increasing from 0.6 to 200 µmol l^{-1} while the bulk sediment [Mo] increases (from 2.1 to 9.6 µg g^{-1}). Romaniello et al. (2016) showed that Mo-enriched Bahamas carbonates ([Mo] 1-10 µg g^{-1}) deposited under high pore-water $[H_2S]_{aq}$ can record δ^{98}Mo values close to seawater. However, as observed in this study and in the case of Romaniello et al. (2016), there may be an Δ^{98}Mo offset of ~-0.5‰ between the seawater and bulk sediments even at high pore-water [H_2S]. In contrast, in Malo Jezero the δ^{98}Mo composition is approaching seawater in the anoxic carbonate-rich sediments with low pore-waters [H_2S] (<< 11 µmol l^{-1}) situated close to the sediment surface (Figure 10 and 11). A few samples from core C2 are characterized with the highest δ^{98}Mo near the seawater composition. The more variable $\delta^{98}Mo_{auth}$ in core C2, compared to C1, may be a consequence of the closer vicinity to the chemocline in the lake and more variable redox conditions within the pore-waters. However, neither pore-water [H_2S] nor other trace metal data for core C2 is available, limiting a more detailed discussion. Core C3 is characterized with the lowest $[Mo]_{bulk}$ and $\delta^{98}Mo_{bulk}$ and the Mo is dominated by the (detrital) carbonate/dolomite fraction with a δ^{98}Mo near ~+1.1‰. Overall, the data suggest that pore-water [H_2S] during early diagenetic processes is critical for authigenic Mo uptake, as also suggested for Bahamas bank carbonate-rich sediments (Romaniello et al. 2016), while Mo uptake associated directly with organic matter or Fe-Mn shuttle processes appear secondary in this setting. Clearly, further work is warranted to identify the link between the pore-water environment, the host of authigenic Mo and isotope fractionation mechanisms in anoxic carbonate-rich sediments.

7. Conclusions

The geochemistry of the carbonate-dominated sediment samples in Malo Jezero are recording the significant documented changes in water column redox conditions. In the deepest part of core C1 (>20 cm depth), high authigenic Mo and U accumulation are consistent with euxinic bottom-water conditions during sediment deposition. Both the $\delta^{98}Mo_{auth}$ (~+1.6‰) and $\delta^{238}U_{auth}$ (~-0‰) are different from the seawater composition, showing similar systematics as observed in Saanich Inlet and Cariaco Basin organic carbon-rich sediments. These observations are consistent with U and Mo uptake from euxinic deep water and pore-water, in a basin with relatively fast deep-water renewal rates. In the shallower part of the same core, both Mo and U uptake likely occurred from a reducing pore-water environment leading to lower authigenic Mo and U accumulation. While the $\delta^{238}U_{auth}$ is relatively similar to the deeper section, the $\delta^{98}Mo_{auth}$ (1.1 to 2.3‰) is more variable, primarily linked to variable pore-water [H_2S].

The results from Malo Jezero show similar δ^{98}Mo and δ^{238}U as recorded within the Bahamas bank carbonate-rich sediments (Chen et al. 2018; Romaniello et al. 2013; Tissot et al. 2018). The results here are generally in accordance with reported shift in bulk sedimentary δ^{238}U towards higher values due to the diagenetic processes of U uptake from reducing pore-waters. The Δ^{238}U between the bulk δ^{238}U carbonate-rich sediments and seawater (+0.31 ± 0.01‰) is slightly higher, but within uncertainty of suggestions based on Bahamas samples (+0.27 ± 0.14‰ (Chen et al. 2018) and +0.24 ± 0.06‰, (Tissot et al. 2018)). If such a Δ^{238}U is used as a 'correction factor' for obtaining seawater compositions in paleo-redox studies, it is important to consider the exact

deposition environment of the samples (oxic vs. anoxic pore-waters) and that the bulk $\delta^{238}U$ is a mixture of authigenic and detrital derived U. The results also suggest that $\delta^{98}Mo$ in carbonate-rich sediments can, under certain conditions, be similar to seawater, however, further work is needed to understand the processes controlling the $\delta^{98}Mo$ in carbonate-rich sediments and its potential as a paleo-redox proxy.

Acknowledgements

This work was supported by the Croatian Science Foundation project IP-2018-01-7813, REDOX and the European Union Seventh Framework Programme (FP7 2007-2013) under grant agreement no. 291823 Marie Curie FP7-PEOPLE-2011-COFUND as part of the project ‘‘Using lakes to develop isotopic tools for understanding ocean redox through Earth history (IsotopicRedoxTools)”. We would like to thank the editor and two anonymous reviewers for insightful comments that improved the interpretations of the manuscript.

References

Abshire, M.L., Romaniello, S.J., Kuzminov, A.M., Cofrancesco, J., Severmann, S., Riedinger, N., 2020. Uranium isotopes as a proxy for primary depositional redox conditions in organic-rich marine systems. Earth Planet. Sci. Lett. 529, p.115878

Algeo, T.J., Lyons, T.W., 2006. Mo-total organic carbon covariation in modern anoxic marine environments: implications for analysis of paleoredox and paleohydrographic conditions. Paleoceanography 21, PA1016. https://doi.org/10.1029/2004PA001112

Alego, T.J., Tribovillard, N., 2009. Environmental analysis of paleoceanographic systems based on molybdenum-uranium covariation. Chem. Geol. 268, 211-225. https://doi.org/10.1016/j.chemgeo.2009.09.001

Allison, L.E., Moodie, C.D., 1965. Carbonate. In: Black, C.A. (Ed.), Methods of Soil Analysis, Part 2, second ed., pp. 1379-1400 Agronomy Monography 9 ASA, CSSA and SSSA.

Amini, M., Weis, D., Soon, M., Francois, R., 2016. Molybdenum Isotope Fractionation in Saanich Inlet, British Columbia. Goldschmidt Conference, Yokohama, *60*. https://goldschmidtabstracts.info/2016/60.pdf

Anbar, A.D., Rouxel, O., 2007. Metal stable isotopes in paleoceanography. Annu. Rev. Earth Planet. Sci. 35, 717-746. https://doi.org/10.1146/annurev.earth.34.031405.125029

Andersen, M.B., Stirling, C.H., Zimmermann, B., Halliday, A.N., 2010. Precise determination of the open ocean $^{234}U/^{238}U$ composition. Geochem. Geophys. Geosyst. 11, 1-8. https://doi.org/10.1029/2010GC003318

Andersen, M.B., Romaniello, S., Vance, D., Little, S.H., Herdman, R., Lyons, T.W., 2014. A modern framework for the interpretation of $^{238}U/^{235}U$ in studies of ancient ocean redox. Earth Planet. Sci. Lett. 400, 184-194. https://doi.org/10.1016/j.epsl.2014.05.051

Andersen, M.B., Vance, D., Morford, J.L., Bura-Nakić, E., Breitenbach, S.F.M., Och, L., 2016. Closing in on the marine $^{238}U/^{235}U$ budget. Chem. Geol. 420, 11-22. https://doi.org/10.1016/j.chemgeo.2015.10.041

Andersen, M.B., Stirling, C.H., Weyer, S., 2017. Uranium isotope fractionation. Rev. Mineral. Geochem. 82, 799–850. https://doi.org/10.2138/rmg.2017.82.19

Andersen, M.B., Matthews, A., Vance, D., Bar-Matthews, M., Archer, C., de Souza, G.F., 2018. A 10-fold decline in the deep Eastern Mediterranean thermohaline overturning circulation during the last interglacial period. Earth Planet. Sci. Lett. 503, 58-67. https://doi.org/10.1016/j.epsl.2018.09.013

Asael, D., Tissot, F.L., Reinhard, C.T., Rouxel, O., Dauphas, N., Lyons, T.W., Ponzevera, E., Liorzou, C., Chéron, S., 2013. Coupled molybdenum, iron and uranium stable isotopes as oceanic paleoredox proxies during the Paleoproterozoic Shunga Event. Chem. Geol. 362, 193-210. https://doi.org/10.1016/j.chemgeo.2013.08.003

Arnold, G.I., Anbar, A.D., Barling, J., Lyons, T.W., 2004. Molybdenum isotope evidence for widespread anoxia in mid-proterozoic oceans. Science 304, 87-90. https://doi.org/10.1126/science.1091785

Azrieli-Tal, I., Matthews, A., Bar-Matthews, M., Almogi-Labin, A., Vance, D., Archer, C., Teutsch, N., 2014. Evidence from molybdenum and iron isotopes and molybdenum-uranium covariation for sulphidic bottom waters during Eastern Mediterranean sapropel S1 formation. Earth Planet. Sci. Lett. 393, 231–242. https://doi.org/10.1016/j.epsl.2014.02.054

Barling, J., Arnold, G.L., Anbar, A.D., 2001. Natural mass-dependent variations in the isotopic composition of molybdenum. Earth Planet. Sci. Lett. 193, 447-457. https://doi.org/10.1016/S0012-821X(01)00514-3

Barling, J., Anbar, A.D., 2004. Molybdenum isotope fractionation during adsorption by manganese oxides. Earth Planet. Sci. Lett. 217, 315–329. https://doi.org/10.1016/S0012-821X(03)00608-3

Barnes, C.E., Cochran, J.K., 1990. Uranium removal in oceanic sediments and the oceanic-U balance. Earth Planet. Sci. Lett. 97, 94-101. https://doi.org/10.1016/0012-821X(90)90101-3

Benović, A., Lučić, D., Onofri, V., Peharda, M., Carić, M., Jasprica, N., Bobanović-Ćolić, S., 2000. Ecological characteristic of the Mljet Island seawater lakes (South Adriatic Sea) with special reference to their resident populations of medusae. Sci. Mar. 64 (Suppl. A), 197-206. http://scimar.icm.csic.es/scimar/pdf/64/sm64s1197.pdf

Brennecka, G.A., Herrmann, A.D., Alego, T.J., Anbar, A.D., 2011. Rapid expansion of oceanic anoxia immediately before the end-Permian mass extinction. Proc. Natl. Acad. Sci. 108, 17631-17634. https://doi.org/10.1073/pnas.1106039108

Buljan, M., Špan, J., 1976. Hydrographical properties of the sea water lakes on the island of Mljet and the adjoining sea in the Eastern South Adriatic Sea. Acta Adriat. VI (12), 1-224 (in Croatian).

Bura-Nakić, E., Andersen, M.B., Archer, D., de Souza, G.F., Marguš, M., Vance, D., 2018. Coupled Mo-U abundances and isotopes in a small marine euxinic basin: Constraints on processes in euxinic basins. Geochim. Cosmochim. Acta 222, 212-222. https://doi.org/10.1016/j.gca.2017.10.023

Chen, X., Ling, H.F., Vance, D., Shields-Zhou, G.A., Zhu, M., Poulton, S.W., Och, L.M., Jiang, S.Y., Li, D., Cremonese, L., Archer, C., 2015. Rise to modern levels of ocean oxygenation coincided with the Cambrian radiation of animals. Nature communications 6, 1-7. https://doi.org/10.1038/ncomms8142

Chen, X., Romaniello, S.J., Herrmann, A.D., Wasylenki, L.E., Anbar, A.D., 2016. Uranium isotope fractionation during coprecipitation with aragonite and calcite. Geochim. Cosmochim. Acta 188, 189-207. https://doi.org/10.1016/j.gca.2016.05.022

Chen, X., Romaniello, S.J., Herrmann, A.D., Hardisty, D., Gill, B.C., Anbar, A.D., 2018. Diagenetic effects on uranium isotope fractionation in carbonate sediments from the Bahamas. Geochim. Cosmochim. Acta 237, 294-311. https://doi.org/10.1016/j.gca.2018.06.026

Cuculić, V., Cukrov, N., Kwokal, Ž., Mlakar, M., 2009. Natural and anthropogenic sources of Hg, Cd, Pb, Cu and Zn in seawater and sediment of Mljet National Park, Croatia. Estuarine, Coastal and Shelf Science 81, 311-320. https://doi.org/10.1016/j.ecss.2008.11.006

Czaja, A.D., Johnson, C.M., Roden, E.E., Beard, B.L., Vogelin, A.R., Nägler, T.F., Beukes, N.J., Wille, M., 2012. Evidence for free oxygen in the Neoarchean ocean based on coupled iron-molybdenum isotope fractionation. Geochim. Cosmochim. Acta 86, 118-137. https://doi.org/10.1016/j.gca.2012.03.007

Dahl, T.W., Hammarlund, E.U., Anbar, A.D., Bond, D.F.G., Gill, B.C., Gordon, G.W., Knoll, A.H., Nielsen, A.T., Schovsbo, N.H., Canfield, D.E., 2010. Devonian rise in atmospheric oxygen correlated to the radiations of terrestrial plants and large predatory fish. PNAS 42, 17911-17915. https://doi.org/10.1073/pnas.1011287107

Dahl, T.W., Boyle, R.A., Canfield, D.E., Connely, J.N., Gill, B.C., Lenton, T.M., Bizzaro, M., 2014. Uranium isotopes distinguish two geochemically distinct stages during the later Cambrian SPICE event. Earth Planet. Sci. Lett. 401, 313-326. https://doi.org/10.1016/j.epsl.2014.05.043

Dickson, A.J., Cohen, A.S., Coe, A.L., 2014. Continental margin molybdenum isotope signatures from the early Eocene. Earth Planet. Sci. Lett. 404, 389–395. https://doi.org/10.1016/j.epsl.2014.08.004

Dickson, A.J., 2017. A molybdenum-isotope perspective on Phanerozoic deoxygenation events. Nature Geoscience 10, 721-726. http://dx.doi.org/10.1038/ngeo3028

Dunk, R.M., Mills, R.A., Jenkins, W.J., 2002. A reevaluation of the oceanic uranium budget for the Holocene. Chem. Geol. 190, 45–67. https://doi.org/10.1016/S0009-2541(02)00110-9

Erickson, B.E., Helz, G.R., 2000. Molybdenum (VI) speciation in sulphidic waters: stability and lability of thiomolybdates. Geochim. Cosmochim. Acta 64, 1149-1158. https://doi.org/10.1016/S0016-7037(99)00423-8

Goldberg, T., Archer, C., Vance, D., Poulton, S. W., 2009. Mo isotope fractionation during adsorption to Fe (oxyhydr)oxides. Geochim. Cosmochim. Acta 73, 6502–6516. https://doi.org/10.1016/j.gca.2009.08.004

Goldberg, T., Archer, C., Vance, D., Thamdrup, B., McAnena, A., Poulton, S.W., 2012. Controls on Mo isotope fractionations in a Mn-rich anoxic marine sediment, Gullmar Fjord, Sweden. Chem. Geol. 296–297, 73–82. https://doi.org/10.1016/j.chemgeo.2011.12.020

Goldberg, T., Poulton, S.W., Wagner, T., Kolonic, S.F., Rehkämper, M., 2016. Molybdenum drawdown during Cretaceous Oceanic Anoxic Event 2. Earth Planet. Sci. Lett. 440, 81-91. https://doi.org/10.1016/j.epsl.2016.02.006

Helz, G.R., Miller, C.V., Charnock, J.M., Mosselmans, J.F.W., Pattrick, R.A.D., Garner, C.D., Vaughan, D.J., 1996. Mechanism of molybdenum removal from the sea and its concentration in black shales: EXAFS evidence. Geochim. Cosmochim. Acta 60, 3631-3642. https://doi.org/10.1016/0016-7037(96)00195-0

Helz, G. R., Bura-Nakić, E., Mikac, N., Ciglenečki, I., 2011. New model for molybdenum behaviour in euxinic waters. Chem. Geol. 284, 323–332. https://doi.org/10.1016/j.chemgeo.2011.03.012

Helz, G.R., Vorlicek, T., 2019. Precipitation of molybdenum from euxinic waters and the role of organic matter. Chem. Geol. 509, 178-193. https://doi.org/10.1016/j.chemgeo.2019.02.001

Jasprica, N., Viličić, D., Carić, M., Njire, J., 1995. Phytoplankton in the Malo and Veliko jezero (island of Mljet, southern adriatic). In: Durbešić, P., Benoviić, A. (Eds.), Proceedings of the Symposium “Natural Characteristic and Social Valorization of the Island of Mljet”. Croatian Ecological Society, Zagreb, pp. 453-463.

Kendall, B., Komiya, T., Lyons, T.W., Bates, S.M., Gordon, G.W., Romaniello, S.J., Jiang, G., Creaser, R.A., Xiao, S., McFadden, K., Sawaki, Y., 2015. Uranium and molybdenum isotope evidence for an episode of widespread ocean oxygenation during the late Ediacaran Period. Geochim. Cosmochim. Acta 156, 173–193. https://doi.org/10.1016/j.gca.2015.02.025

Kendall, B., Dahl, T.W., Anbar, A.D., 2017. The stable isotope geochemistry of molybdenum. Reviews in Mineralogy and Geochemistry, 82(1), 683-732. https://doi.org/10.2138/rmg.2017.82.16

Kerl, C.F., Lohmayer, R., Bura-Nakić, E., Vance, D., Planer-Friedrich, B., 2017. Experimental confirmation of isotope fractionation in thiomolybdates using ion chromatography and detection by multi-collector ICP-MS. Anal. Chem. 89, 3123-3129. https://doi.org/10.1021/acs.analchem.6b04898

King, E.K., Perakis, S.S., Pett-Ridge, J.C., 2018. Molybdenum isotope fractionation during adsorption to organic matter. Geochim. Cosmochim. Acta 222, 584-598. https://doi.org/10.1016/j.gca.2017.11.014

Klinkhammer, G.P., Palmer, M.R., 1991. Uranium in the oceans: where it goes and why. Geochim. Cosmochim. Acta 55, 1799-1806. https://doi.org/10.1016/0016-7037(91)90024-Y

Kowalski, N., Dellwig, O., Beck, M., Gräwe, U., Neubert, N., Nägler, T.F., Badewien, T.H., Brumsack, H.J., van Beusekom, J.E.E., Böttcher, M.E., 2013. Pelagic molybdenum concentration anomalies and the impact of sediment resuspension on the molybdenum budget in two tidal

systems of the North Sea. Geochim. Cosmochim. Acta 119, 198-211. https://doi.org/10.1016/j.gca.2013.05.046

Lojen, S., Sondi, I., Juračić, M., 2010. Geochemical conditions for the preservation of recent aragonite-rich sediments in Mediterranean karstic marine lakes (Mljet Island, Adriatic Sea, Croatia). Marine and Freshwater Research 61, 119-128. https://doi.org/10.1071/MF09034

Lovley, D.R., Phillips, E.J.P., Gorby Y.A., Landa E.R., 1991. Microbial reduction of uranium. Nature 350, 413–416. https://do.org/10.1038/350413a0

Lyons, T.W., Reinhard, C.T., Planavsky, N.J., 2014. The rise of oxygen in Earth's early atmosphere. Nature 506, 307-315. https://doi.org/10.1038/nature13068

McManus, J., Berelson, W.M., Klinkhammer, G.P., Hammond, D.E., Holm, C., 2005. Authigenic uranium: relationship to oxygen penetration depth and organic carbon rain. Geochim. Cosmochim. Acta 69, 95–108. https://doi.org/10.1016/j.gca.2004.06.023

McManus, J., Berelson, W.M., Severmann, S., Poulson, R.L., Hammond, D.E., Klinkhammer, G.P., Holm, C., 2006. Molybdenum and uranium geochemistry in continental margin sediments: paleoproxy potential. Geochim. Cosmochim. Acta 70(18), 4643-4662. https://doi.org/10.1016/j.gca.2006.06.1564

Montoya-Pino, C., Weyer, S., Anbar, A.D., Pross, J., Oschmann, W., van de Schootbrugge, B., Arz, H.W., 2010. Global enhancement of ocean anoxia during Anoxic Oceanic Event 2: A quantitative approach using U isotopes. Geology 38, 315-318. https://doi.org/10.1130/G30652.1

Morford, J.L., Emerson, S.R., Breckel, E.J., Kim, S.H., 2005. Diagenesis of oxyanions (V, U, Re, and Mo) in pore waters and sediments from a continental margin. Geochim. Cosmochim. Acta 69(21), 5021-5032. https://doi.org/10.1016/j.gca.2005.05.015

Nägler, T.F., Neubert, N., Böttcher, M.E., Dellwig, O., Schnetger, B., 2011. Molybdenum isotope fractionation in pelagic euxinia: Evidence from the modern Black and Baltic Seas. Chem. Geol. 289, 1-11. https://doi.org/10.1016/j.chemgeo.2011.07.001

Nägler T. F., Anbar A. D., Archer C., Goldberg T., Gordon G. W., Greber N. D., Siebert C., Sohrin Y., Vance D., 2014. Proposal for an international molybdenum isotope measurement standard and data representation. Geostand. Geoanal. Res. 38, 149–151. https://doi.org/10.1111/j.1751-908X.2013.00275.x

Nakagawa, Y., Takano, S., Firdaus, M.L., Norisuye, K., Hirata, T., Vance, D., Sohrin, Y., 2012. The molybdenum isotopic composition of the modern ocean. Geochem. J. 46, 131-141. https://doi.org/10.2343/geochemj.1.0158

Noordmann, J., Weyer, S., Montoya-Pino, C., Dellwig, O., Neubert, N., Eckert, S., Paetzel, M., Böttcher, M.E., 2015. Uranium and molybdenum isotope systematics in modern euxinic basins: Case studies from the central Baltic Sea and the Kyllaren fjord (Norway). Chem. Geol. 396, 182-195. https://doi.org/10.1016/j.chemgeo.2014.12.012

Planavsky, N.J., Reinhard, C.T., Wang, X., Thomson, D., McGoldrick, P., Rainbird, R.H., Johnson, T., Fischer, W.W., Lyons, T.W., 2014. Low Mid-Proterozoic atmospheric oxygen levels and the delayed rise of animals. Science 346, 635-638. https://doi.org/10.1126/science.1258410

930 Poulson, R.L., Siebert, C., McManus, J., Berelson, W.M., 2006. Authigenic molybdenum isotope
931 signatures in marine sediments. Geology 34, 617–620. https://doi.org/10.1130/G22485.1

932 Poulson Brucker, R.L., McManus, J., Severmann, S., Berelson, W.M., 2009. Molybdenum
933 behavior during early diagenesis: Insights from Mo isotopes. Geochem. Geophys. Geosyst. 10,
934 1-25. https://doi.org/10.1029/2008GC002180

935 Rolison, J.M., Stirling, C.H., Middag, R., Rijkenberg, M.J.A., 2017. Uranium stable isotope
936 fractionation in the Black Sea: Modrn calibration of the $^{238}U/^{235}U$ paleo-redox proxy. Geochim.
937 Cosmochim. Acta 203, 69-88. https://doi.org/10.1016/j.gca.2016.12.014

938 Romaniello, S.J., Hermann, A., Anbar, A.D., 2013. Uranium concentrations and $^{238}U/^{235}U$ isotope
939 ratios in modern carbonates from the Bahamas: Assessing a novel paleoredox proxy. Chemical
940 Geology 362, 305-316. https://doi.org/10.1016/j.chemgeo.2013.10.002

941 Romaniello, S.J., Hermann, A., Anbar, A.D., 2016. Syndepositional diagenetic control of
942 molybdenum isotope variations in carbonate sediments from the Bahamas. Chemical Geology
943 438, 84-90. https://doi.org/10.1016/j.chemgeo.2016.05.019
944
945 Russell, A.D., Morford, J.L., 2001. The behaviour of redox-sensitive metals across a laminated -
946 massive-laminated transition in Saanich Inlet, British Columbia. Marine Geology 174, 341-354.
947 https://doi.org/10.1016/S0025-3227(00)00159-6

948 Scholz, F., Siebert, C., Dale, A.W., Frank, M., 2017. Intense molybdenum accumulation in
949 sediments underneath a nitrogenous water column and implications for the reconstruction of
950 paleo-redox conditions based on molybdenum isotopes. Geochm. Cosmochim. Acta 213, 400-
951 417. https://doi.org/10.1016/j.gca.2017.06.048
952
953 Schubert, R. (1909) Geologischer Führer durch Dalmatien. Sammlung Geologischer Führer 24,
954 Berlin.

955 Siebert, C., Nägler, T.F., Kramers, J.D., 2001. Determination of molybdenum isotope fractionation
956 by double-spike multicollector inductively coupled plasma mass spectrometry. Geochemistry,
957 Geophysics, Geosystems 2, 2000GC000124. https://doi.org/10.1029/2000GC000124

958 Siebert, C., Nägler, T.F., von Blanckenburg, F., Kramers, J.D., 2003. Molybdenum isotope
959 records as a potential new proxy for paleoceanography. Earth Planet. Sci. Lett. 211, 159-171.
960 https://doi.org/10.1016/S0012-821X(03)00189-4

961 Sondi, I., Juračić, M., 2010. Whiting events and the formation of aragonite in Mediterranean
962 Karstic Marine Lakes: new evidence on its biologically induced inorganic origin. Sedimentology
963 57, 85-95. https://doi.org/10.1111/j.1365-3091.2009.01090.x

964 Sondi, I., Mikac, N., Vdović, N., Ivanić, M., Furdek, M., Škapin, S.D., 2017. Geochemistry of recent
965 aragonite-rich sediments in Mediterranean karstic marine lakes: Trace elements as pollution and
966 palaeoredox proxies and indicators of authigenic mineral formation. Chemosphere 168, 786-797.
967 http://dx.doi.org/10.1016/j.chemosphere.2016.10.134

968 Stirling, C.H., Andersen, M.B., Potter, E.-K., Halliday, A.N., 2007. Low temperature isotopic
969 fractionation of uranium. Earth Planet. Sci. Lett. 264, 208–225.
970 https://doi.org/10.1016/j.epsl.2007.09.019

971 Telus, M., Dauphas, N., Moynier, N., Tissot, F.L.H., Teng, F.Z., Nabelek, P.I., Craddock, P.R.,
972 Groat, L.A., 2012. Iron, zinc, magnesium and uranium isotopic fractionation during continental
973 crust differentiation: the tale from migmatites, granitoids, and pegmatites. Geochim. Cosmochim.
974 Acta 97, 247–265. https://doi.org/10.1016/j.gca.2012.08.024

975 Tossell, J.A., 2005. Calculating the partitioning of the isotopes of Mo between oxidic and sulfidic
976 species in aqueous solution. Geochim. Cosmochim. Acta 69, 2981-2993.
977 https://doi.org/10.1016/j.gca.2005.01.016

978 Tissot, F.L.H., Chen, C., Go, B.M., Nazeimiec, M., Healy, G., Bekker, A., Swart, P.L., Dauphas,
979 N., 2018. Controls of eustasy and diagenesis on the $^{238}U/^{235}U$ of carbonates and evolution of the
980 seawater ($^{234}U/^{238}U$) during the last 1.4 Myr. Geochim. Cosmochim. Acta 242, 233-265.
981 https://doi.org/10.1016/j.gca.2018.08.022

982 Vilibić, I., Žuljević, A., Nikolić, V., 2010. The dynamics of a saltwater marine lake (Big Lake, Island
983 of Mljet, Adriatic Sea) as revealed by temperature measurements. Acta Adriat. 51, 119-130.
984 https://hrcak.srce.hr/64361

985 Vogelin, A.R., Nägler, T.F., Samankassou, E., Villa, I.M., 2009. Molybdenum isotopic composition
986 of modern and Carboniferous carbonates. Chem. Geol. 265, 488-498.
987 https://doi.org/10.1016/j.chemgeo.2009.05.015

988 Voegelin, A.R., Nägler, T.F., Beukes, N.J., Lacassie, J.P., 2010. Molybdenum isotopes in late
989 Archean carbonate rocks: Implications for early Earth oxygenation. Precambrian Research 182(1-
990 2), 70-82. https://doi.org/10.1016/j.precamres.2010.07.001

991 Vuletić, A., 1953. Geological structure of the bottom of Malo and Veliko jezero on the island of
992 Mljet. Acta Adriat. VI(1), 1-65 (in French).

993 Zheng, Y., Anderson, R.F., van Geen, A., Fleisher, M.Q., 2002. Preservation of particulate non-
994 lithogenic uranium in marine sediments. Geochim. Cosmochim. Acta 66, 3085-3092.
995 https://doi.org/10.1016/S0016-7037(01)00632-9

996 Wagner, M., Chappaz, A., Lyons, T.W., 2017. Molybdenum speciation and burial pathway in
997 weakly sulfidic environments: Insights from XAFS. Geochim. Cosmochim. Acta 206, 18-29.
998 https://doi.org/10.1016/j.gca.2017.02.018

999 Wasylenki, L.E., Rolfe, B.A., Weeks, C.L., Spiro, T.G., Anbar, A.D., 2008. Experimental
1000 investigation of the effects of temperature and ionic strength on Mo isotope fractionation during
1001 adsorption to manganese oxides. Geochim. Cosmochim. Acta 72, 5997–6005.
1002 https://doi.org/10.1016/j.gca.2008.08.027

1003 Weyer, S., Anbar, A.D., Gerdes, A., Gordon, G.W., Alego, T.J., Boyle, E.A., 2008. Natural
1004 fractionation of $^{238}U/^{235}U$. Geochim. Cosmochim. Acta 72, 345-359.
1005 https://doi.org/10.1016/j.gca.2007.11.012

1006 Wunsam, S., Schmidt, R., Müller, J., 1999. Holocene lake development of two Dalmatian lagoons
1007 (Malo and Veliko Jezero, isle of Mljet) in respect to changes in Adriatic Sea level and climate.
1008 Paleogeogr. Paleoclimatol. Paleoecol. 146, 251-281. http://dx.doi.org/10.1016/S0031-
1009 0182(98)00147-3ž

1010

Table captions (within text)

Table 1. Bulk sedimentary (cores C1, C2 and C3) Mo and U isotopic composition ($\delta^{98}Mo_{bulk}$ and $\delta^{238}U_{bulk}$) as well and $(^{234}U/^{238}U)_{act}$ in Malo Jezero sediments.

Table 2. Sedimentary (cores C1, C2 and C3) authigenic Mo and U compositions ($\delta^{98}Mo_{auth}$ and $\delta^{238}U_{auth}$) and concentration ($[Mo]_{auth}$ and $[U]_{auth}$) in Malo Jezero sediments.

Figure captions

Figure 1. Location of Mljet Island, Croatia, in the Adriatic Sea and the Malo and Veliko Jezero at the western tip of the Island. The sediment sampling locations are indicated at lake depths of 30 meter (core C1), 22 meter (core C2), and 13 meter (core C3).

Figure 2. Vertical distribution of trace elements (Al, Ti, Sr, V, Mo and U) in Malo Jezero sediments for cores C1 (blue triangles), C2 (green circles) and C3 (red squares). The vertical distribution of $CaCO_3$ content (wt%) (data for C1 core are taken from Sondi et al. (2017)) and of bulk sedimentary $\delta^{98}Mo$, $\delta^{238}U$ and $(^{234}U/^{238}U)_{act}$ is also shown.

Figure 3. $[Al]_{bulk}$ vs $[Ti]_{bulk}$, $[Li]_{bulk}$, $[Sr]_{bulk}$, $[Mo]_{bulk}$, $[U]_{bulk}$, $[V]_{bulk}$ as well as $[Sr]_{bulk}$ vs $[Mo]_{bulk}$, $[U]_{bulk}$, $[V]_{bulk}$ covariation in Malo Jezero sediments for cores C1 (blue triangles), C2 (green circles) and C3 (red squares). The detrital limestone/dolomite (grey) and soil siliciclastic (yellow) end-members are marked as rhombs. The limestone/dolomite end-member represents an average of five samples while the soil-endmember is based on the *terra rossa* sample.

Figure 4. $(^{234}U/^{238}U)_{act}$ covariation with $[Sr]_{bulk}$ (A) and with $1/[U]_{bulk}$ (B) for Malo Jezero sediments in cores C1 (blue triangles), C2 (green circles) and C3 (red squares). The *terra rossa* and dolomite/limestone (top sample in core C3) detrital end-members are shown as yellow and grey rhomb, respectively. The green cross is the measured $(^{234}U/^{238}U)_{act}$ in the lake waters (average of 1.137). Arrow represent a two-component mixing estimate.

Figure 5. Uranium (A) and Mo (B) to Al cross-plots for cores C1 (blue triangles), C2 (green circles) and C3 (red squares) and detrital dolomite/limestone 'rock' (grey rhombs) and soil '*terra rossa'* (yellow rhombs) end-members. Mixing lines between the detrital end-members are also shown. The mixing lines are used to calculate the relative authigenic vs. detrital fraction of each sample, visualized by the vertical vector line for one sample in A). Plot C) is a zoom in from B) in the lower [Mo] range.

Figure 6. Depth profiles of authigenic [Mo] and [U] as well as the authigenic $\delta^{98}Mo$ and $\delta^{238}U$ for Malo Jezero sediments for cores C1 (blue triangles), C2 (green circles) and C3 (red squares).

Figure 7. The authigenic $\delta^{238}U$ vs. [U] and authigenic $\delta^{98}Mo$ vs. [Mo] for cores C1 (blue triangles), C2 (green circles) and C3 (red squares). The sediment samples from below and above 20 cm depth in cores C1 and C2, are shown as open and filled symbols, respectively. Average $\delta^{238}U$ offsets from the seawater $\delta^{238}U$ composition for these two groups of data, are shown in the authigenic $\delta^{238}U$ vs. [U] plot.

Figure 8. Bulk [Mo] (A) and [U] (B) vs. C_{org} (wt %) correlation within core 1 (C_{org} data from Lojen et al. (2010)). The data shown no clear correlations, however the data from <20 cm show a weak negative correlation between both [Mo] (A) and [U] (B) vs. C_{org} (see text for further discussion). A similar trend in the data is observed plotting authigenic, instead of bulk, Mo and U.

Figure 9. Plots of $\delta^{238}U_{auth}$ vs. $1/[U]_{auth}$(ppm), $\delta^{98}Mo_{auth}$ vs. $1/[Mo]_{auth}$(ppm), $\delta^{238}U_{auth}$ vs. $[U]_{auth}$(ppm)/C_{org} (Wt.%) and $\delta^{98}Mo_{auth}$ vs. $[Mo]_{auth}$(ppm)/ C_{org} (Wt.%). Mixing relationships between different sources of authigenic Mo and U accumulations may be expressed as linear correlations in the diagrams (see main text for further discussion).

Figure 10. U vs Mo enrichment factors (A) and authigenic $\delta^{98}Mo$ vs $\delta^{238}U$ (B) for Malo Jezero sediments compared to the average estimates of other modern euxinic basins (from Bura-Nakić et al. 2018 and references therein). The sediment samples from below and above 20 cm depth in cores C1 and C2 are shown as open and filled symbols, respectively. The grey squares represent average estimates for core C1 below (grey square with red cross) and above (grey square with blue cross) 20 cm depth, in (A) and (B). The colored circles represent sediment data from other restricted basins as labelled in diagram B. The arrows within diagram B indicates low Mo/U versus high Mo/U uptake (from Bura-Nakić et al. 2018).

Figure 11. Depth profiles of pore-water H_2S (orange), Mo (blue) and Fe (blue) and Mn (orange) concentrations for core C1. Depth profiles of sedimentary $\delta^{98}Mo_{auth}$ and $[Mo]_{auth}$ are also shown. In parallel is a simplified model for $\delta^{98}Mo_{auth}$ accumulation divided into the three zones: *i*) zone of Mn-oxide and Fe-oxyhydroxides dissolution; *ii*) zone of sedimentary Mo uptake from pore-waters and *iii*) zone of previous Mo uptake from within euxinic bottom-waters. Within zone *i*) the mixing of Mo sources with the different isotopic compositions may lead to low $\Delta^{98}Mo$. Zone ii) is characterized with shallow zone of sedimentary Mo uptake in the form of MoO_4^{2-} accompanied with minor $\Delta^{98}Mo$ and a deeper zone of the sedimentary Mo uptake accompanied with the more expressed $\Delta^{98}Mo$, likely due to the non-quantitative transformation of MoO_4^{2-} to the MoS_4^{2-}. Zone *iii*) is characterized with Mo uptake from within a euxinic water column at the time of deposition, accompanied with $\Delta^{98}Mo$ of ~-0.7‰ compared to seawater (see text for further discussion).

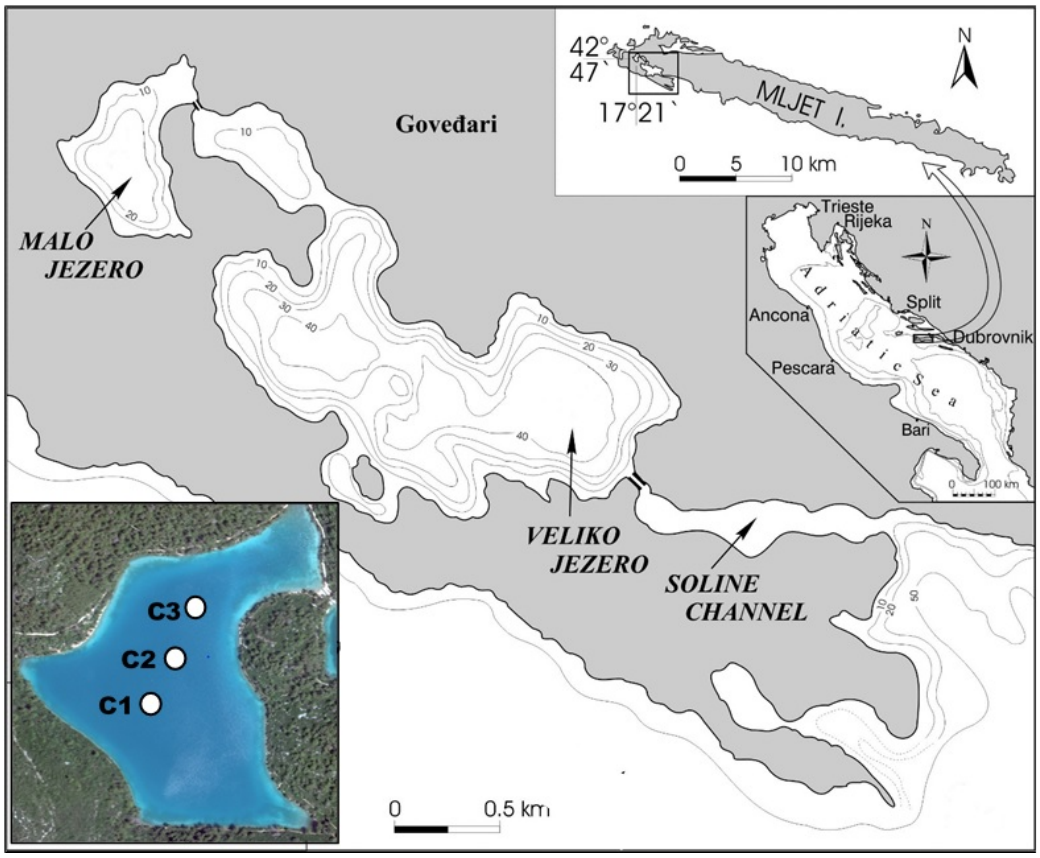
Goveđari
MALO
JEZERO
VELIKO
JEZERO
SOLINE
CHANNEL
42°
47`
17°21`
MLJET I.
0 5 10 km
N
Trieste
Rijeka
Ancona
Split
Dubrovnik
Pescara
Bari
Adriatic Sea
0 100 km
C3
C2
C1
0 0.5 km

1085

1086

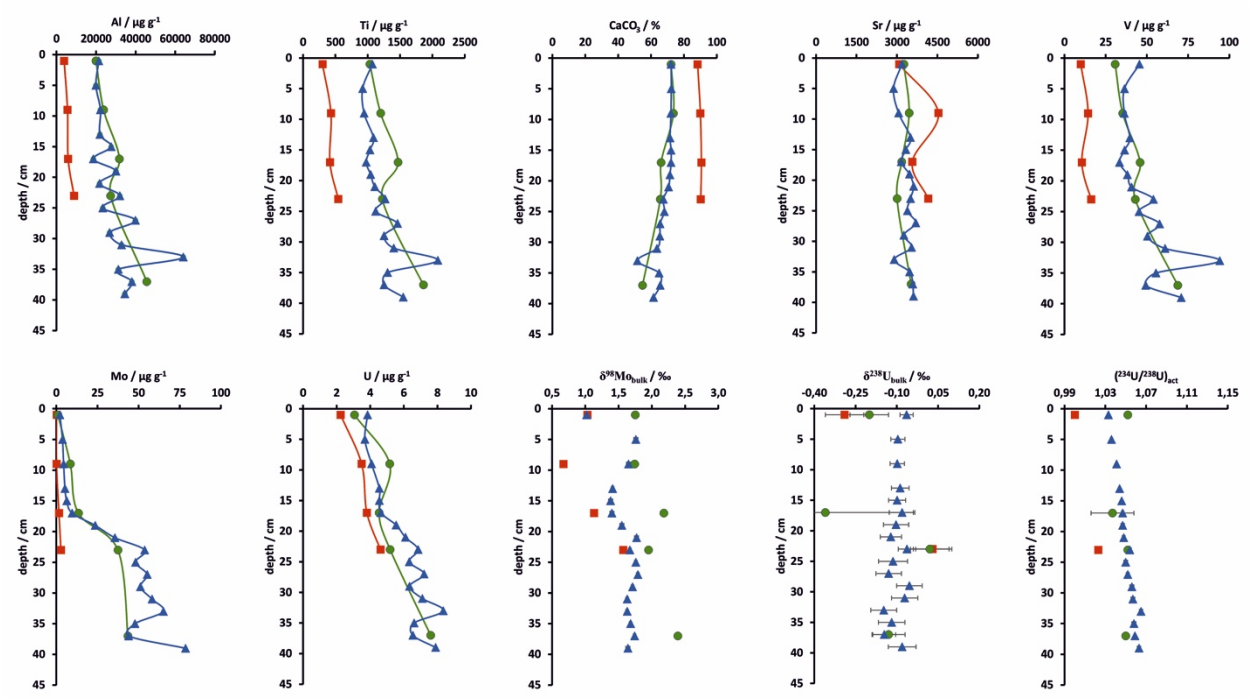
Al / µg g-1
Ti / µg g-1
CaCO3 / %
Sr / µg g-1
V / µg g-1
Mo / µg g-1
U / µg g-1
δ98Mobulk / ‰
δ238Ubulk / ‰
(234U/238U)act
depth / cm

1087

1088

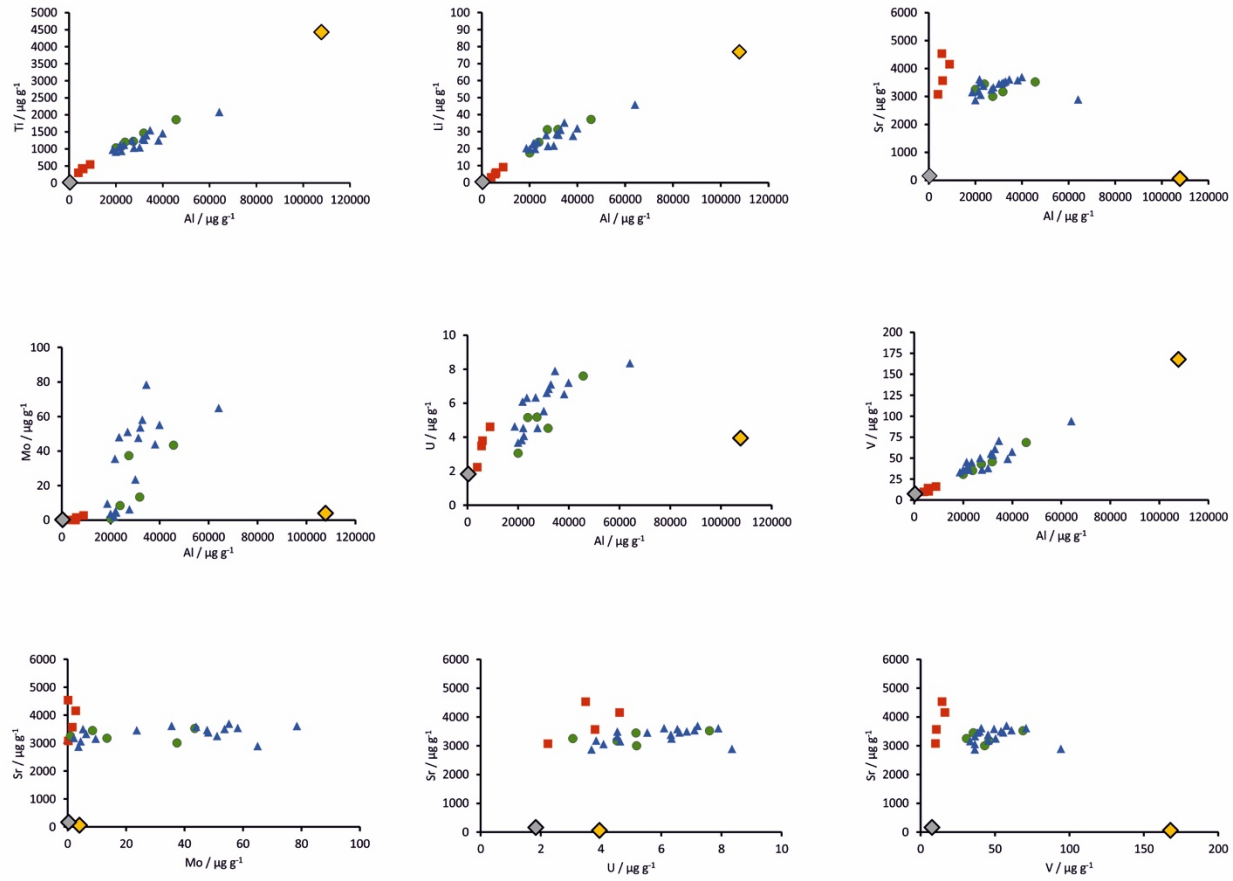

1089

1090

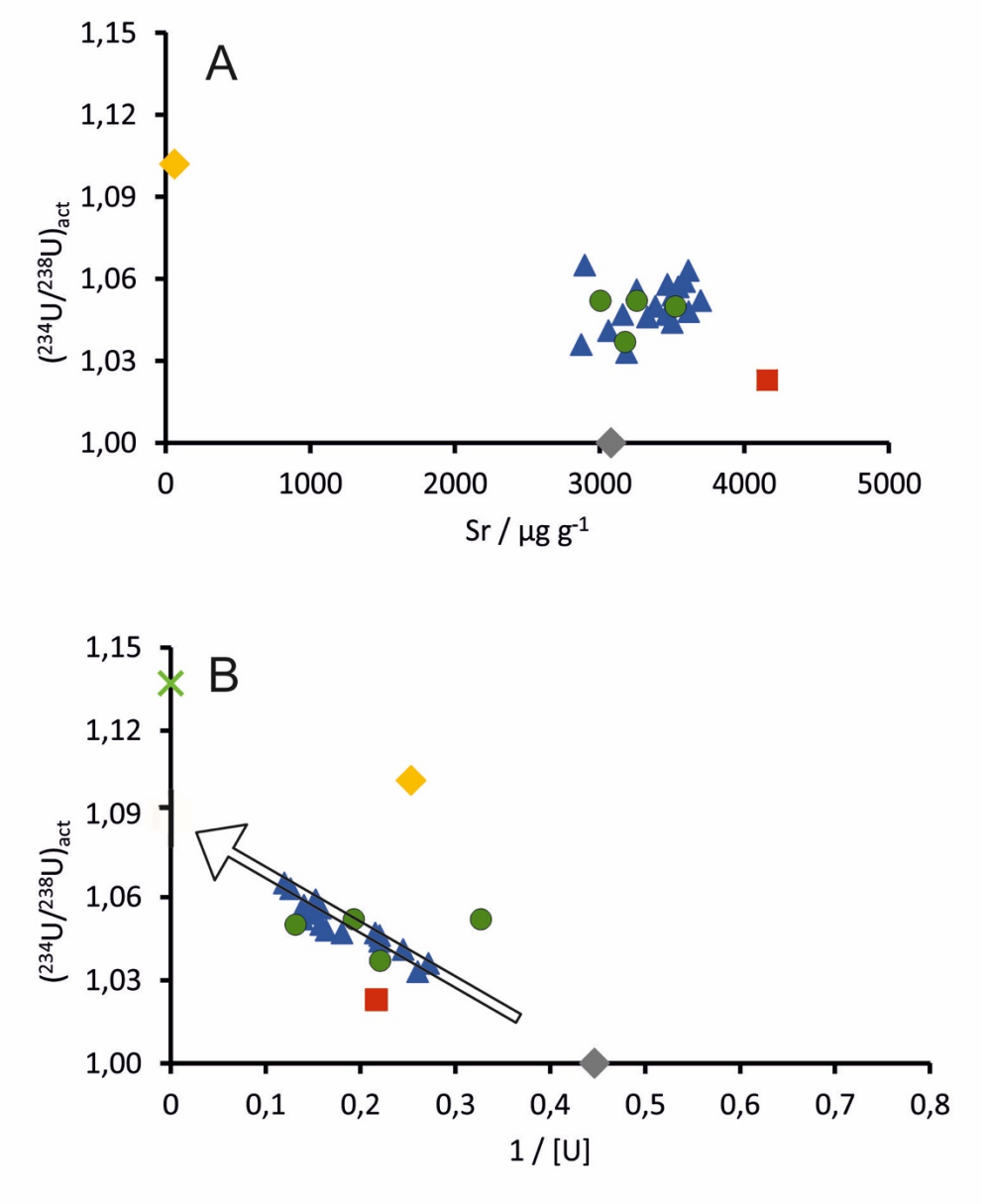
A
1,15
1,12
1,09
1,06
1,03
1,00
(234U/238U)act
0
1000
2000
3000
4000
5000
Sr / µg g-1
B
1,15
1,12
1,09
1,06
1,03
1,00
(234U/238U)act
0
0,1
0,2
0,3
0,4
0,5
0,6
0,7
0,8
1 / [U]

1091

1092

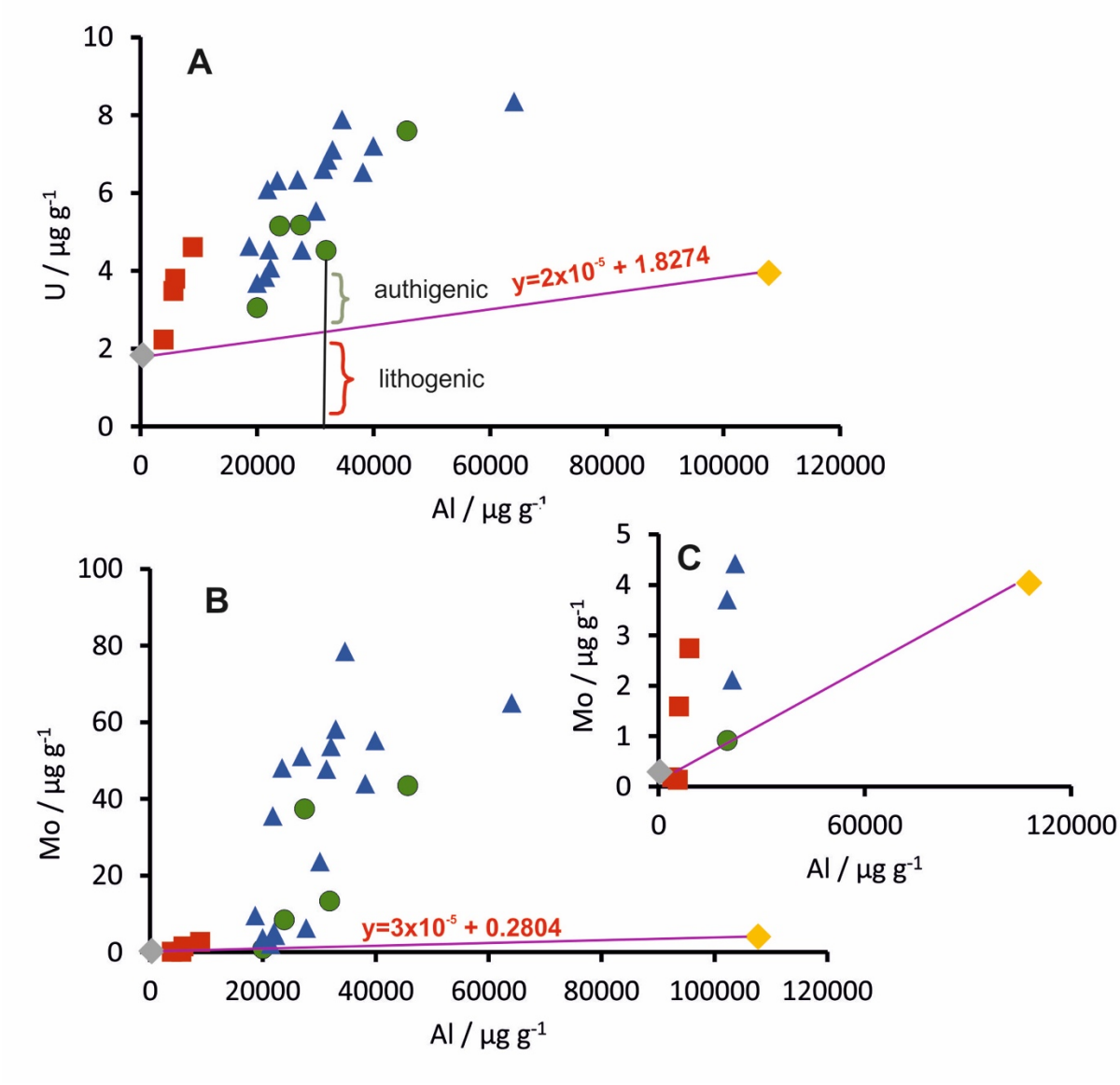
A
U / µg g-1
Al / µg g-1
authigenic
lithogenic
y=2x10-5 + 1.8274
B
Mo / µg g-1
Al / µg g-1
y=3x10-5 + 0.2804
C
Mo / µg g-1
Al / µg g-1

1093

1094

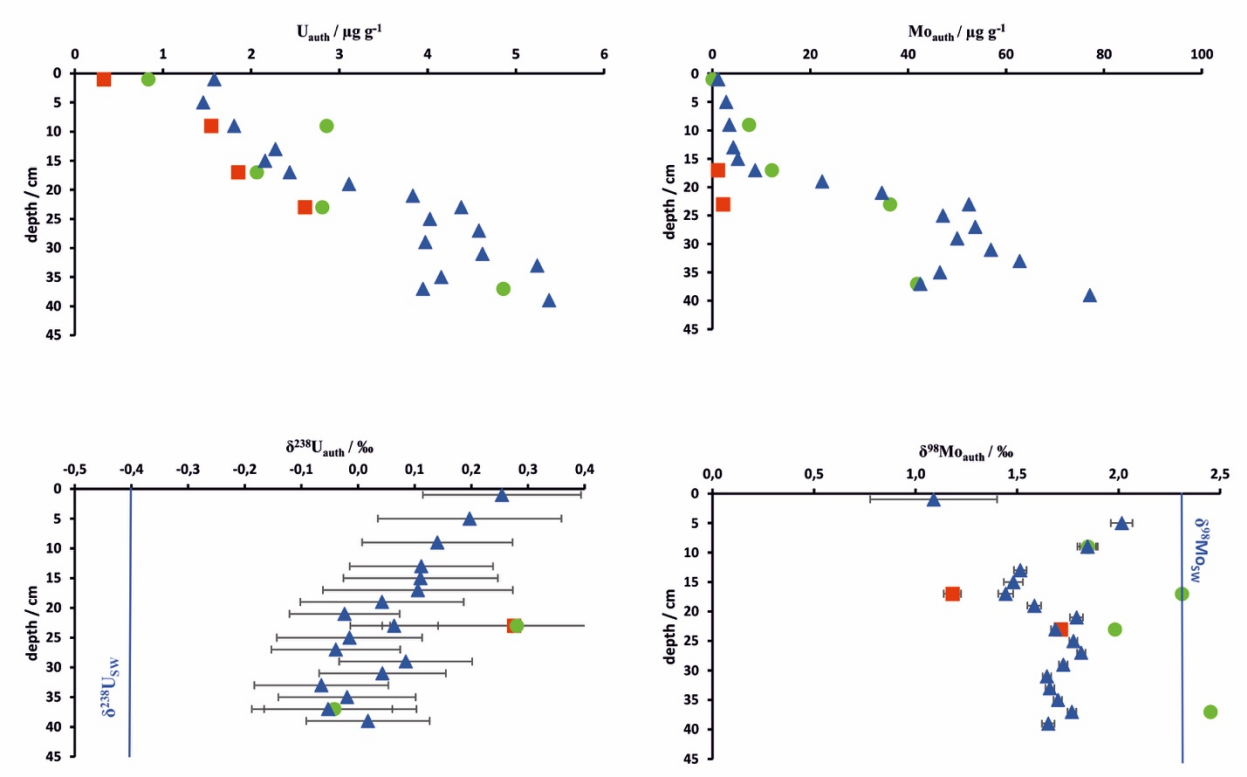
U_auth / µg g-1
Mo_auth / µg g-1
depth / cm
δ238U_auth / ‰
δ98Mo_auth / ‰
δ238USW
δ98MoSW

1095

1096

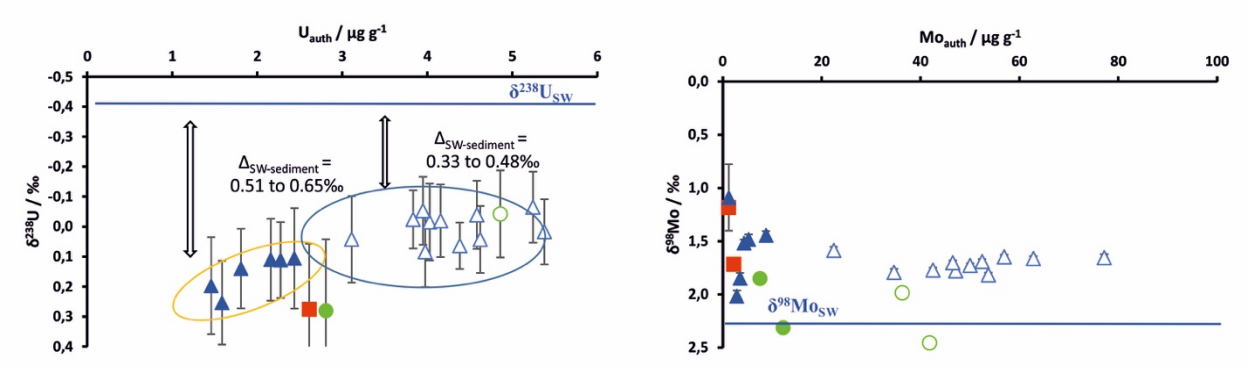
U_auth / µg g-1
0
1
2
3
4
5
6
-0,5
-0,4
-0,3
-0,2
-0,1
0,0
0,1
0,2
0,3
0,4
δ238U / ‰
δ238USW
ΔSW-sediment =
0.51 to 0.65‰
ΔSW-sediment =
0.33 to 0.48‰
Moauth / µg g-1
0
20
40
60
80
100
0,0
0,5
1,0
1,5
2,0
2,5
δ98Mo / ‰
δ98MoSW

1097

1098

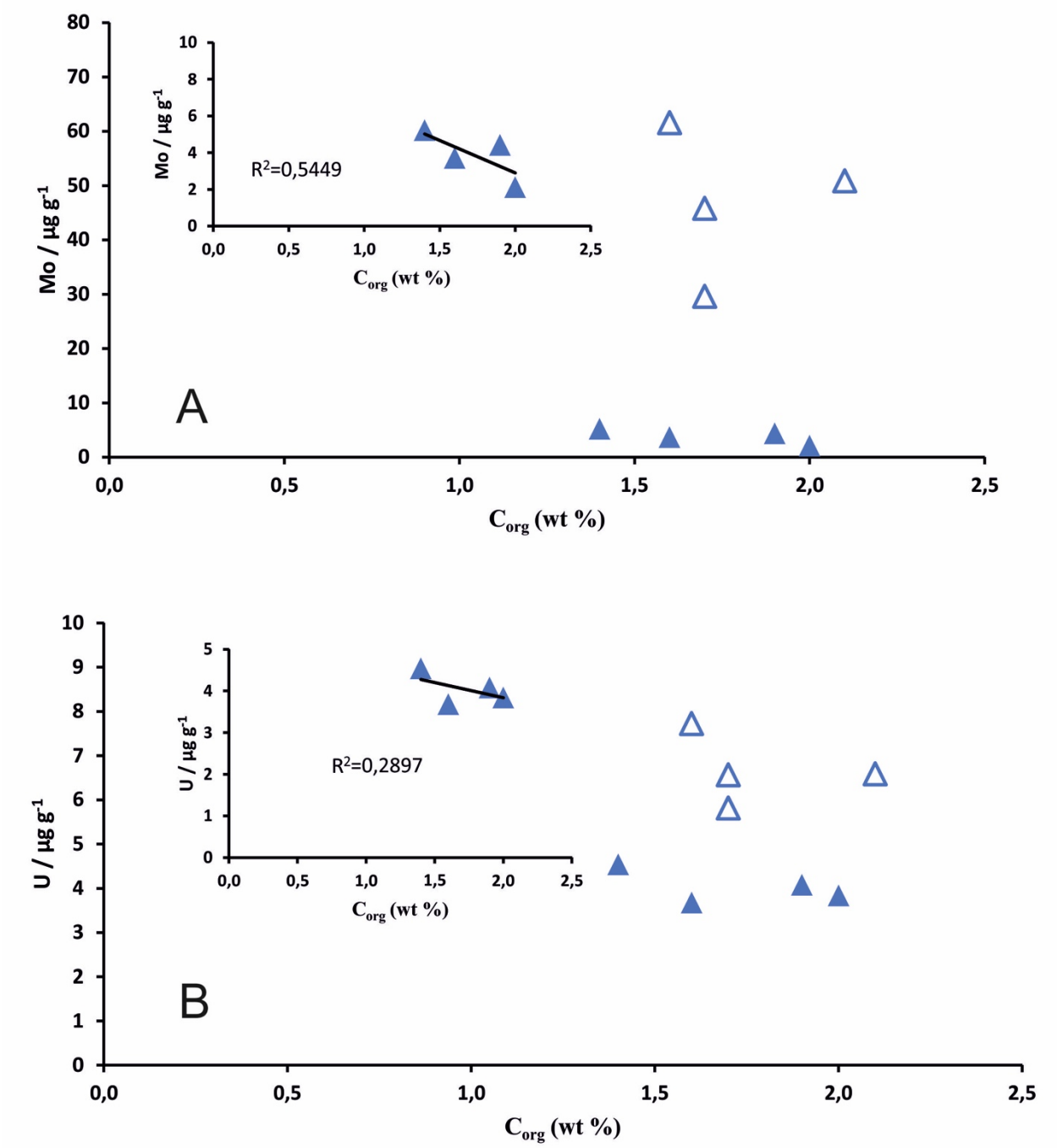
Mo / µg g-1
80
70
60
50
40
30
20
10
0
0,0
0,5
1,0
1,5
2,0
2,5
Corg (wt %)
A
Mo / µg g-1
10
8
6
4
2
0
R2=0,5449
0,0
0,5
1,0
1,5
2,0
2,5
Corg (wt %)
U / µg g-1
10
9
8
7
6
5
4
3
2
1
0
0,0
0,5
1,0
1,5
2,0
2,5
Corg (wt %)
B
U / µg g-1
5
4
3
2
1
0
R2=0,2897
0,0
0,5
1,0
1,5
2,0
2,5
Corg (wt %)

1099

1100

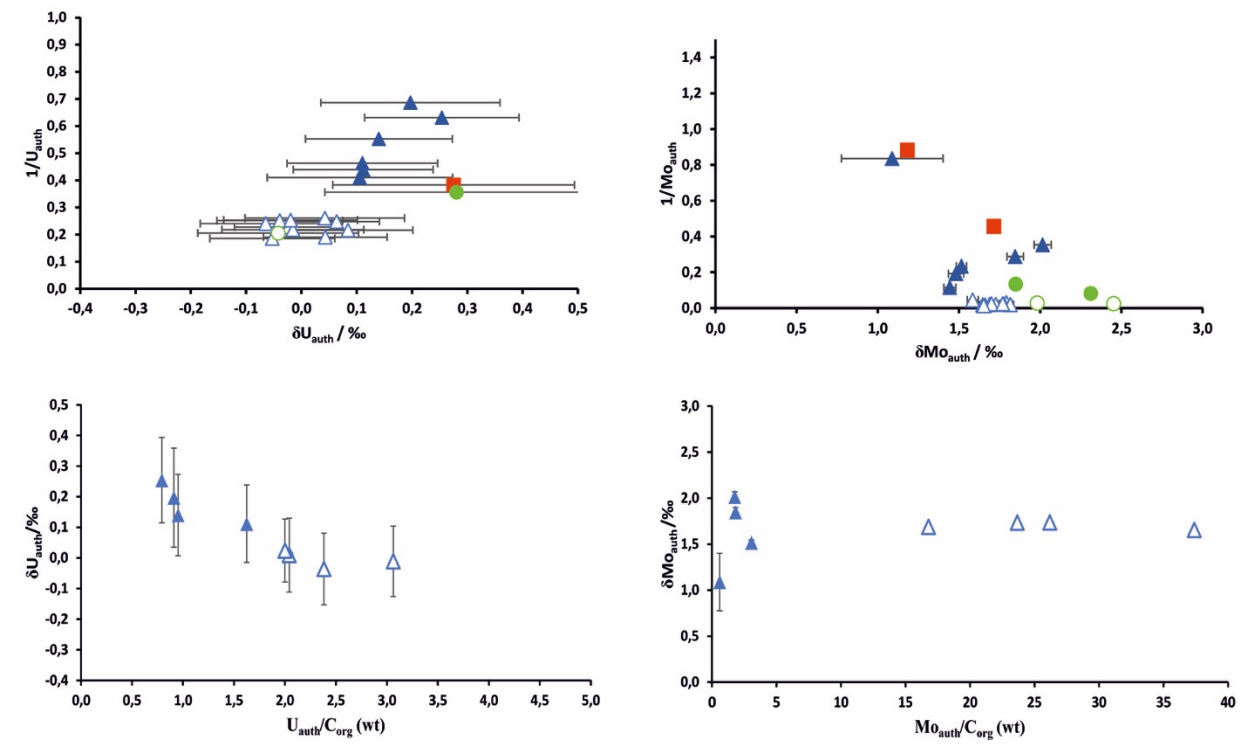
1/Uauth
δUauth / ‰
1/Moauth
δMoauth / ‰
δUauth/‰
Uauth/Corg (wt)
δMoauth/‰
Moauth/Corg (wt)

1101

1102

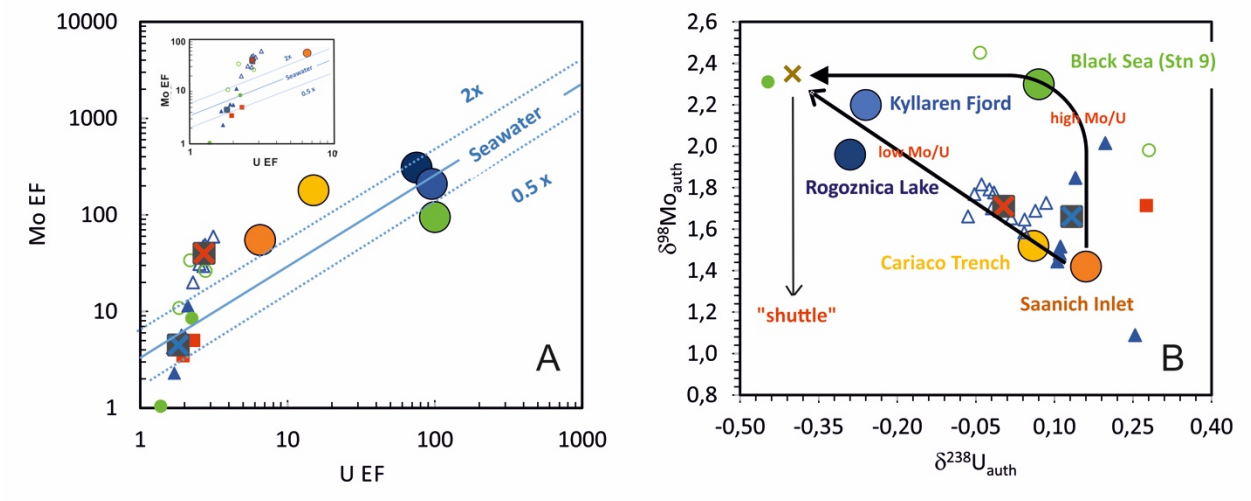
Mo EF
U EF
2x
Seawater
0.5 x
A
Black Sea (Stn 9)
Kyllaren Fjord
high Mo/U
low Mo/U
Rogoznica Lake
Cariaco Trench
Saanich Inlet
"shuttle"
B
δ98Moauth
δ238Uauth

1103

1104

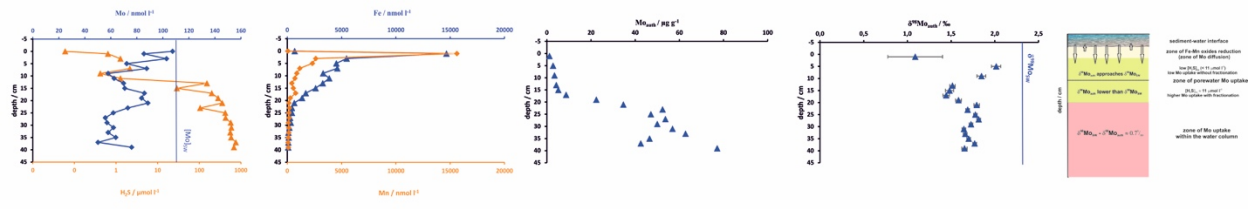
Mo / nmol l-1
depth / cm
H2S / µmol l-1
Fe / nmol l-1
Mn / nmol l-1
Momob / pg g-1
δ98Momob / ‰
sediment-water interface
zone of Fe-Mn oxides reduction (zone of Mo diffusion)
zone of porewater Mo uptake
zone of Mo uptake within the water column

1105

1106

Table 1. Sedimentary Mo and U bulk isotopic composition ($\delta^{98}Mo_{bulk}$ and $\delta^{238}U_{bulk}$) as well $(^{234}U/^{238}U)_{act}$ in Malo Jezero sediments within cores C1, C2 and C3. The same data is given for the catchment soil samples (*terra rossa* and humus soil).

	Depth /cm	$\delta^{98}Mo_{bulk}$/‰	± 2σ	$\delta^{238}U_{bulk}$/‰	± 2σ	$(^{234}U/^{238}U)_{act}$	± 2σ
Core C3	1	1,03	0,05	-0,29	0,07	1,000	0,003
	9	0,67	0,07	-	-	-	-
	17	1,13	0,02	-	-	-	-
	23	1,57	0,02	0,03	0,07	1,023	0,003
Core C2	1	1,75	0,03	-0,20	0,07	1,052	0,003
	9	1,74	0,03	-	-	-	-
	17	2,18	0,02	-0,36	0,32	1,037	0,021
	23	1,95	0,02	0,02	0,07	1,052	0,003
	37	2,39	0,02	-0,13	0,06	1,050	0,003
Core C1	1	1,02	0,03	-0,06	0,02	1,033	0,000
	5	1,76	0,03	-0,10	0,03	1,036	0,001
	9	1,65	0,03	-0,10	0,03	1,041	0,001
	13	1,41	0,02	-0,09	0,03	1,044	0,001
	15	1,38	0,03	-0,10	0,03	1,046	0,001
	17	1,40	0,03	-0,08	0,05	1,047	0,001
	19	1,55	0,03	-0,10	0,05	1,047	0,002
	21	1,77	0,03	-0,12	0,04	1,048	0,001
	23	1,67	0,02	-0,06	0,03	1,054	0,001
	25	1,76	0,02	-0,11	0,05	1,050	0,002
	27	1,79	0,02	-0,13	0,05	1,052	0,001
	29	1,71	0,02	-0,05	0,05	1,056	0,001
	31	1,63	0,02	-0,07	0,05	1,057	0,002
	33	1,63	0,02	-0,15	0,05	1,065	0,002
	35	1,68	0,02	-0,12	0,05	1,058	0,002
	37	1,74	0,02	-0,15	0,04	1,059	0,000
	39	1,64	0,03	-0,08	0,05	1,063	0,002
Soil (*terra rossa*)		0,53	0,03	-0,28	0,22	1,102	0,003
Soil (humus soil)		0,62	0,04	-0,22	0,12	0,977	0,003

Table 2. Sedimentary Mo and U authigenic isotopic composition ($\delta^{98}Mo_{auth}$ and $\delta^{238}U_{auth}$) and authigenic concentration ($[Mo]_{auth}$ and $[U]_{auth}$) in Malo Jezero sediments within cores C1, C2 and C3.

	Depth / cm	U_{auth}/µg g^{-1}	Mo_{auth}/µg g^{-1}	$\delta^{238}U_{auth}$/‰	± 2σ	$\delta^{98}Mo_{auth}$/‰	± 2σ
Core C3	1	0,33	n/a*	-0,30	4.20	n/a*	
	9	1,55	n/a*	-	-	n/a*	
	17	1,85	1,13	-	-	1,18	0,04
	23	2,61	2,19	0,28	0,22	1,72	0,03
Core C2	1	0,83	0,04	0,04	0,92	20,2	19,0
	9	2,86	7,5	-	-	1,85	0,04
	17	2,07	12,2	-0.45	0.40	2,31	0,02
	23	2,81	36,3	0,28	0,24	1,98	0,02
	37	4,86	41,8	-0,04	0,14	2,45	0,02
Core C1	1	1,58	1,20	0,25	0,14	1,09	0,31
	5	1,46	2,83	0,20	0,16	2,02	0,05
	9	1,81	3,48	0,14	0,13	1,85	0,05
	13	2,27	4,29	0,11	0,13	1,52	0,03
	15	2,16	5,21	0,11	0,14	1,48	0,05
	17	2,44	8,74	0,11	0,17	1,44	0,04
	19	3,11	22,4	0,04	0,14	1,58	0,03
	21	3,83	34,7	-0,02	0,10	1,79	0,03
	23	4,38	52,4	0,06	0,08	1,69	0,02
	25	4,03	47,1	-0,01	0,13	1,78	0,02
	27	4,58	53,7	-0,04	0,11	1,82	0,02
	29	3,98	50,0	0,08	0,12	1,73	0,02
	31	4,62	56,9	0,04	0,11	1,65	0,02
	33	5,24	62,8	-0,07	0,12	1,66	0,02
	35	4,16	46,5	-0,02	0,12	1,70	0,02
	37	3,95	42,5	-0,05	0,11	1,77	0,02
	39	5,38	77,2	0,02	0,11	1,65	0,03

*The detrital fraction of $[Mo]_{bulk}$ too dominant to calculate an authigenic fraction.

Supplementary Table 1. H_2S concentrations in Malo Jezero water column from 1951 to 1961 (Data taken from Buljan and Špan, 1976).

Year	Date	Lake depth / m	
		20	25
		H_2S / mg l^{-1}	H_2S / mg l^{-1}
1951	13.03.	not detected	1,86
	19.04.	not detected	3,72
	18.05.	not detected	2,21
	17.06.	not detected	2,22
	13.07.	0,61	3,31
	24.08.	0,33	2,96
	04.10.	1,32	2,73
	07.11.	not detected	2,53
	13.12.	not detected	2,35
1952	15.01.	not detected	2,88
	21.02.	not detected	4,71
	06.03.	not detected	3,88
	31.03.	not detected	3,01
	02.04.	not detected	1,93
	05.05.	not detected	3,43
	07.05.	present	2,88
	08.06.	present	present
	10.06.	present	present
	15.07.	present	present
	17.07.	present	present
	19.08.	present	present
	21.08.	not detected	present
	25.09.	not detected	present
	27.09.	not detected	3,17
	06.11.	1,28	2,33
	08.11.	not detected	traces
	11.12.	4,84	4,95
	13.12.	3,83	3,68
1953	22.01.	not detected	traces
	05.03.	not detected	2,93
	19.05.	pink water, not detected	not detected
	21.05.	pink water, not detected	not detected
	24.06.	red water, traces	no data
	14.08.	present	no data
	16.08.	present	present
	23.09.	2,93	3,21
	24.11.	not detected	0,20

1954	20.01.	not detected	not detected
	12.03.	not detected	not detected
	27.05.	not detected	not detected
	21.07.	not detected	not detected
	20.08.	not detected	not detected
	25.09.	not detected	not detected
	24.11.	not detected	1,12
1955	13.02.	not detected	not detected
	01.04.	not detected	not detected
	25.09.	present	present
1956	02.03.	not detected	1,48
1961	12.07.	not detected	not detected

1124

Table 2. Vertical distribution of trace elements (Al, Ti, Li, Sr, Mo, U and V) and $CaCO_3$ content in Malo Jezero sediments within cores C1, C2 and C3.

Sediment	Depth /cm	Al / µg g^{-1}	Ti / µg g^{-1}	Li / µg g^{-1}	$CaCO_3$ / %	Sr / µg g^{-1}	Mo_{bulk} / µg g^{-1}	U_{bulk} / µg g^{-1}	V_{bulk} / µg g^{-1}
Core C3	1	3895	301	3	88,3	3078	0,2	2,2	9,9
	9	5587	431	5	90,0	4536	0,1	3,5	14,3
	17	5926	416	6	90,6	3569	1,6	3,8	10,5
	23	8902	544	9	90,2	4158	2,7	4,6	16,2
Core C2	1	19968	1032	18	72,2	3256	0,9	3,1	30,7
	9	23808	1199	24	73,6	3451	8,5	5,2	35,3
	17	31814	1468	31	66,1	3175	13,4	4,5	45,9
	23	27404	1225	31	65,6	3004	37,4	5,2	43,0
	37	45642	1860	37	54,8	3524	43,5	7,6	68,7
Core C1	1	21403	1072	23	72,2	3185	2,1	3,8	45,5
	5	19966	921	20	72,3	2874	3,7	3,7	36,4
	9	22254	944	20	72,1	3062	4,4	4,1	36,3
	13	22011	1088	23	71,6	3501	5,2	4,5	39,6
	15	27673	1034	22	72,2	3330	6,3	4,5	36,5
	17	18641	976	20	72,2	3159	9,5	4,6	33,4
	19	30107	1044	22	71,5	3462	23,6	5,5	38,2
	21	21769	1109	23	70,7	3615	35,6	6,1	40,7
	23	32078	1268	28	67,5	3505	53,7	6,9	54,0
	25	23439	1122	24	68,1	3386	48,1	6,3	45,3
	27	39927	1460	32	65,5	3697	55,2	7,2	57,7
	29	26919	1252	28	65,4	3256	51,1	6,3	50,4
	31	32930	1402	31	63,6	3543	58,2	7,1	61,0
	33	64093	2084	46	51,7	2896	65,0	8,4	94,2
	35	31317	1306	29	64,9	3468	47,7	6,6	55,5
	37	38155	1251	28	65,6	3586	43,4	6,5	49,3
	39	34548	1549	35	61,5	3613	78,5	7,9	70,8

Repeated measurements of BCR–2 gave reproducibilities better than ± 10% (1 S.D.) and mean values within ± 10% of certified concentrations

1131

Supplementary Table 3. Al, Ti, Li, Sr, Mo, V and U concentrations in the catchment Malo Jezero samples.

	Al / µg g^{-1}	Ti / µg g^{-1}	Li / µg g^{-1}	Sr / µg g^{-1}	Mo / µg g^{-1}	U / µg g^{-1}	V / µg g^{-1}
Catchment							
Host rock samples (limestone and dolomite)							
#1	192	11	0,39	125	0,20	1,3	3,5
#2	970	49	1,4	392	0,73	3,6	23,3
#3	169	9	0,27	92	0,19	1,5	3,8
#4	163	9	0,24	92	0,14	1,4	3,7
#5	174	7	0,25	121	0,20	1,4	3,5
Soil samples							
Soil (*terra rossa*)	107752	4431	77	61	4,0	4.0	168
Soil (humus soil)	53395	2323	36	102	1,4	2,4	72

Repeated measurements of BCR–2 gave reproducibilities better than ± 10% (1 S.D.) and mean values within ± 10% of certified concentrations

Supplementary Table 4. Pore-water Mo, U, Fe and Mn concentrations were taken from Sondi et al. (2017) while the porewater [H_2S] was obtained within this study as described within the 'methods' section.

Pore-water	Depth / cm	Mo / nmol l^{-1}	U /nmol l^{-1}	Fe / nmol l^{-1}	Mn / nmol l^{-1}	H_2S / µmol l^{-1}
C1 core	0	107	14,3	1,79	84,2	0,06
	1	86	7,1	12747	13032	0,64
	3	103	4,9	2020,16	4613,29	1,28
	5	72	4,7	1122,62	3319,99	0,00
	7	88	5,7	992,10	2998,50	2,15
	9	58	4,0	796,58	2261,15	0,42
	11	63	8,6	1094,10	1814,27	1,28
	13	70	6,6	650,21	1059,55	153
	15	71	7,0	464,56	860,72	29
	17	86	8,0	444,02	502,15	200
	19	84	8,5	440,12	306,53	284
	21	88	11,7	404,64	241,1	357
	23	73	11,2	118,93	248,19	105
	25	62	8,7	177,76	202,40	422
	27	56	8,3	47,71	128,65	430
	29	57	7,0	94,13	76,41	570
	31	62	9,3	1,79	64,47	592
	33	58	7,7	309,11	128,92	556
	35	64	9,2	1,79	43,12	584
	37	50	9,5	1,79	33,35	755
	39	76	12,1	1,79	48,10	681

Supplementary Table 5. Dissolved Mo and U concentrations and isotope compositinos in the Malo Jezero water column (0, 12 and 25 m depth).

Water column depth	Mo / nmol l^{-1}	U / nmol l^{-1}	$\delta^{98}Mo$/‰	± 2σ	$\delta^{238}U$/‰	± 2σ	$(^{234}U/^{238}U)_{act}$	± 2σ
0 m	105.7	13.4	2,40	0,02	-0,35	0,03	1,138	0,001
12 m	110.2	13.8	2,42	0,02	-0,36	0,02	1,136	0,001
25 m	103.3	13.0	2,42	0,02	-0,37	0,03	1,137	0,001

Supplementary Table 6. Sedimentary lithogenic Mo and U fractions ($[Mo]_{lith}$ and $[U]_{lith}$ – estimated using linear regression equations presented in Figure 3, Mo_{lith}/Al and U_{lith}/Al ratios and estimated Mo and U enrichment factors (Mo_{EF} and U_{EF}).

	Depth /cm	U_{lith} / μg g^{-1}	Mo_{lith} / μg g^{-1}	$U_{litih}/Al \times 10^{-4}$	$Mo_{lith}/Al \times 10^{-4}$	U_{EF}	Mo_{EF}
Core C3	1	1,9	0,4	4,9	1,0	1,2	0,5
	9	1,9	0,5	3,5	0,8	1,8	0,3
	17	2,0	0,5	3,3	0,8	2,0	3,5
	23	2,0	0,6	2,3	0,6	2,3	5,0
Core C2	1	2,2	0,7	1,1	0,4	1,4	1,0
	9	2,3	1,0	1,0	0,4	2,2	8,5
	17	2,5	1,2	0,8	0,4	1,8	10,9
	23	2,4	1,1	0,9	0,4	2,2	33,9
	37	2,7	1,7	0,6	0,4	2,8	26,4
Core C1	1	2,3	0,9	1,1	0,4	1,7	2,3
	5	2,2	0,7	1,1	0,4	1,7	4,2
	9	2,3	1,0	1,0	0,4	1,8	4,7
	13	2,3	0,9	1,0	0,4	2,0	5,6
	15	2,4	1,1	0,9	0,4	1,9	5,7
	17	2,2	0,8	1,2	0,5	2,1	11,4
	19	2,4	1,2	0,8	0,4	2,3	20,0
	21	2,3	0,9	1,0	0,4	2,7	38,1
	23	2,5	1,2	0,8	0,4	2,8	43,2
	25	2,3	1,0	1,0	0,4	2,8	48,9
	27	2,6	1,5	0,7	0,4	2,8	37,4
	29	2,4	1,1	0,9	0,4	2,7	47,0
	31	2,5	1,3	0,8	0,4	2,7	45,9
	33	3,1	2,2	0,5	0,3	2,7	29,5
	35	2,5	1,2	0,8	0,4	2,7	39,1
	37	2,6	1,4	0,7	0,4	2,5	30,8
	39	2,5	1,3	0,7	0,4	3,1	59,6